VARIABLE CONDUCTANCE HEAT PIPE TECHNOLOGY

Final Research Report

MARCH 1974

Prepared by

W. T. ANDERSON
D. K. EDWARDS
J. E. ENINGER
B. D. MARCUS

Contract No. NAS 2-5503

Prepared for

AMES RESEARCH CENTER
NATIONAL AERONAUTICS AND SPACE ADMINISTRATION
Moffett Field, California 93405

TRW
SYSTEMS GROUP

ONE SPACE PARK ● REDONDO BEACH CALIFORNIA 90278

HEAT PIPE TECHNOLOGY Final Research
Report (TRW Systems Group) 87 p
HC $7.50   CSCL 20M   N74-21589

                                        Unclas
                                 G3/33 30274

FORWARD

The work described in this report was performed under NASA Contract NAS 2-5503, "Design, Fabrication and Testing of a Variable Conductance Constant Temperature Heat Pipe". The contract was administered by Ames Research Center, Moffett Field, California, under the technical direction of Mr. J. P. Kirkpatrick.

The program was conducted by TRW Systems Group of TRW, Inc., Redondo Beach, California. Dr. Bruce D. Marcus served as Program Manager. Contributors to the effort described, in addition to the authors, include Messrs. L. Beason, G. Fleischman, P. Mock, D. Opper, G. Patchell, V. Reineking and C. Salts.

TABLE OF CONTENTS

FIGURES

TABLES

25

1.0   INTRODUCTION

For the last several years TRW Systems Group, under contract to NASA-ARC, has performed an extensive research and development program in variable-conductance heat-pipe technology. The treatment has been comprehensive, involving theoretical and/or experimental studies in hydrostatics, hydrodynamics, heat transfer into and out of the pipe, fluid selection, and materials compatibility, in addition to the principal subject of variable-conductance control techniques. Efforts were not limited to analytical work and laboratory experimentation, but extended by the development, fabrication and test of spacecraft hardware, highlighted in the successful flight of the Ames Heat Pipe Experiment on the OAO-C spacecraft.

Most of the program's accomplishments have been previously documented in a series of reports and publications. Early theoretical and design developments appear in References [1-1, 1-2, 1-3, 1-4, 1-5]. Later fundamental work was published in References [1-6, 1-7, 1-8]. Hardware development and application efforts were documented in References [1-9, 1-10, 1-11], and a computer program for designing and predicting performance of gas loaded heat pipes was presented in Reference [1-12].

This document represents the final report on the contract and presents the results of TRW's latest efforts. It does not attempt to present all of the work accomplished on the program, since most has been previously published. However, to provide a summary of the program's scope and a guide as to the location of previously published information, copies of the Tables of Contents of all earlier reports are included in the Appendix.

The particular studies that are covered in this report fall into four areas as follows:

1) An experimental and theoretical study was made of gas generation in methanol/stainless-steel heat pipes for the purpose of establishing a scaling law for the accelerated testing of such heat pipes (Section 2.0).

2) The TRW GASPIPE computer program, previously developed on this contract (Ref.[1-12], was extended to include two condenser sections with different properties, which enables the program to be easily applied to gas-loaded heat pipes having a secondary short condenser (cold trap) adjacent to the gas reservoir as well as an adiabatic section (Section 3).

3) Theoretical and experimental work was carried out on the effect of noncondensable gas on arterial performance. Pressure fluctuations in gas-loaded ammonia heat pipes were studied, and a glass heat pipe was fabricated to study a new method of venting noncondensable gas during priming (Section 4.0).

4) Two research heat pipes (and two spares) were designed, fabricated and tested for a forthcoming GSFC sounding-rocket experiment to study arterial priming in zero gravity. These heat pipes have internal thermistor instrumentation that provides information on the priming process (Section 5.0).

2.0   DEVELOPMENT OF GAS GENERATION SCALING LAWS FOR METHANOL/
          STAINLESS-STEEL HEAT PIPES

Heat pipes are rapidly becoming a serious design element
in the solution of many spacecraft thermal control problems where long
periods of trouble free performance are required. For design purposes,
therefore, there is interest in determining methods for estimating the
operating lifetime. What is meant by "operating lifetime" depends on the
type of heat pipe and the requirements placed on it in a specific appli-
cation. With high temperature liquid metal heat pipes, for example,
structural failure sometimes occur and this is a well-defined termination
of life. In low temperature heat pipes applicable to spacecraft thermal
control, catastrophic failures rarely occur. Instead, heat-pipe performance
continuously degrades as a result of (1) chemical reaction or decomposition
of the working fluid with the generation of noncondensable gas, or (2)
corrosion and erosion of the container and wick.

In an ordinary heat pipe all noncondensable gas is swept to
the condenser end, forming a diffusion barrier to vapor flow and effectively
reducing the available condenser area. In gas controlled, variable conduc-
tance heat pipes, the generation of additional noncondensable gas raises
the operating temperature of the heat pipe above design conditions. Similar
effects can result from a change in the chemical composition of the working
fluid by virtue of a change in its vapor pressure as a function of temperature.

Corrosion and erosion of the container and wick can be manifested
as a change in the wetting angle of the working fluid as well as the
permeability, porosity, or capillary pore size of the wick. Solid
precipitates resulting from corrosion and erosion are transported by the
flowing liquid to the evaporator region where they are deposited when
the liquid vaporizes. This leads to increased resistance to fluid flow
in the evaporator, resulting in a decrease in the heat transport capacity
of the heat pipe.

With these failure mechanisms, where continual degradation
occurs, the operating lifetime can be defined as that period of time beyond
which the operation of the heat pipe is below design specifications. Some
heat pipe laboratories have been performing "life tests" under which heat
pipes are held at normal operating conditions for many thousands of hours

3

to determine the "operating lifetimes". This approach has limited applicability, however, for heat pipes which are required to function well for long periods of time. Progress in heat-pipe development will be impeded if each time a new material combination, fabrication technique, or cleaning procedure is used, life tests of 10,000 hours or more are required. There exists, therefore, a major impetus for understanding the chemical and corrosion mechanisms, and developing scaling laws for the life-limiting processes. The need for achieving very long lived high reliability heat-pipe systems in a rapidly charging technology necessitates the employment of accelerated testing techniques.

This program was the second in a continuing effort to understand compatibility problems as they relate to heat-pipe operating lifetimes. The initial study [2-1, 2-2] in this series was carried out using nickel/water heat pipes as a feasibility demonstration to assess the difficulties in establishing a scaling law relationship for a specific example. From a study of hydrogen evolution in nickel/water heat pipes under accelerated (high) and reference (low) operating conditions it was found possible to accurately predict, with a scaling law, the lifetime of a heat pipe operating at reference conditions from data taken at accelerated conditions. It was also found that the same form of scaling law correlated the data of Petrick [2-3] on stainless-steel/water heat pipes. These results suggested that the formulation of scaling laws for accelerated testing of life-limiting processes is indeed feasible and that similar methods might be applicable to other heat-pipe systems as well.

The present program is concerned with developing scaling laws for gas generation in stainless-steel/methanol heat pipes. Previous life testing of such heat pipes has shown this combination to be compatible up to 145°F (63°C), but gas generation has been observed in these heat pipes at higher temperatures. As stainless-steel/methanol heat pipes represent the most desirable combination for many variable conductance heat pipes, it was important that a study be made of the gas generation behavior at higher temperatures. Before this program was carried out, even the high temperature limit of operation, before the initiation of significant gas generation, was unknown.

4

The primary objective was to formulate an accurate scaling law, based on a chemical and corrosion model of gas evolution mechanisms, for stainless-steel/methanol heat pipes, which predicts the usable lifetime at reference (low) operating conditions from data taken at accelerated (high) operating conditions. This method of accelerated life testing is based on extrapolation from accelerated conditions to predict behavior at reference (normal) conditions. It is thus explicitly ass   't the chemical and physical mechanisms responsible for heat-pipe gradat at accelerated conditions are the same in nature at the reference conditions. Similar ideas are used for other types of accelerated corrosion testing [2-4]. It is emphasized that this work was not concerned with achieving compatibility between stainless steel and methanol. However, strict control was maintained over the starting materials and fabrication techniques, not to eliminate gas generation, but to allow the separation of temperature and fluid circulation effects.

2.1   Accelerated Life Testing

2.1.1   Heat Pipe Materials and Fabrication

Sixteen heat pipes were fabricated using 304 stainless-steel materials. Fabrication procedures which are standard at TRW for construction of stainless-steel/methanol heat pipes were used in order that the results of accelerated life testing would be directly applicable to actual heat pipes built by TRW. Container tubes were 19.5" in length with 1/2" O.D. and 0.020" walls. Two layers of 150 mesh (2.6 mil diameter) screen were installed and the end caps were machined from 1/2" O.D. rods. Closure tubes were cut from 1/8" O.D., 0.020" wall tubing. Care was taken to ensure that all the heat pipes were as nearly t.e same as possible in terms of materials and construction procedures. All containers were cut from 304 stainless steel tube of the same heat number and the same was true of the closure tubing and rods from which the end caps were machined. Screens were cut from a single sheet of wire mesh. Welding was performed with argon in the tube using 308 stainless-steel welding rod and care was taken to use the same temperature and co.. te the weld in the same length of time for each heat pipe. After the screens were installed and the parts cleaned, one end cap was welded, and in this condition all the parts were vacuum fired for 1 hour at $100C°C$ below 10^{-4} torr. The remaining

5

welds were then completed and the heat pipes were filled with 5.5 ml of methanol (Matheson Coleman & Bell, spectroquality grade containing a maximum of 0.05% water) and instrumented with 6" heaters. A schematic diagram of a heat pipe prepared for accelerated testing is shown in Figure 2-1. After filling, one heat pipe was found to be unusable due to excess gas in the pipe, probably resulting from a leak during the filling procedure. All other heat pipes were found to contain initially only a small amount of gas. Eleven copper-constantan thermocouples were placed at 3/4" intervals along the condenser, and one thermocouple was placed in the adiabatic section, for the purpose of measuring the non-condensable gas content by means of the temperature profile. An additional thermocouple was placed on the end cap at the heater end to test for burn-out. Insulation consisted of an inner layer of J-M micro-fibers felt and an outer layer of J-M aerotube.

2.1.2   Measurement of Noncondensable Gas Evolution

As noncondensable gas is evolved during operation of a heat pipe, it is carried to the condenser end causing blockage and a consequent temperature profile along the wall. The amount of gas present may be calculated from the temperature profile assuming ideal gas behavior. If the condenser end is divided into N equal intervals and the temperature at the center of each interval is T_i, then under steady-state condit- the number of lb moles of gas n is given by the ideal gas law as:

$$n = \frac{\Delta V}{R} \sum_{i=1}^{N} \frac{P_{gi}}{T_i} , \qquad (2\text{-}1)$$

where ΔV is the volume of each interval, R is the gas constant, and

$$P_{gi} = P_{va} - P_{vi} \qquad (2\text{-}2)$$

is the partial pressure of gas at the center of the ith interval. In (2-2), P_{va} is the total pressure (the vapor pressure corresponding to the temperature in the adiabatic section) and P_{vi} is the vapor pressure in the ith interval.

A computer program was used to calculate the quantity of gas in a heat pipe at any given time from the measured steady-state wall temperature profile. This method is based on the assumption that the
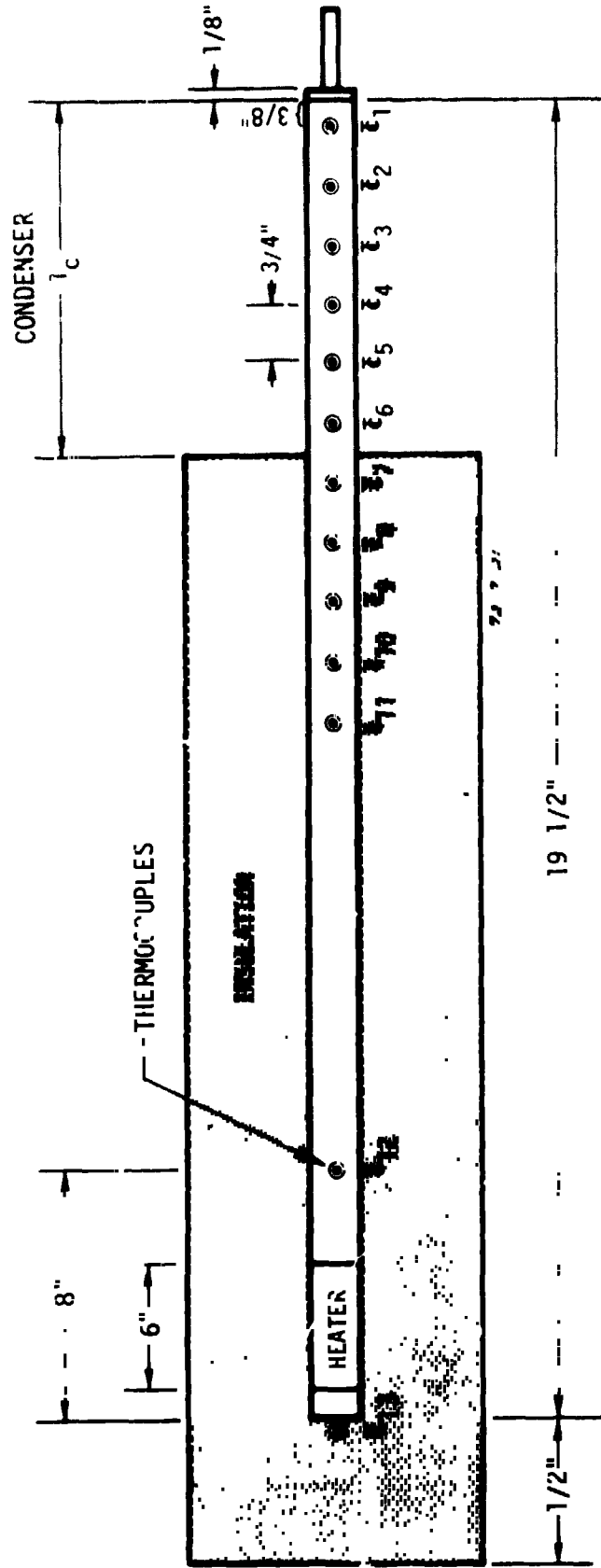
FIGURE 2.7. Schematic Diagram of Heat Pipes Subjected to Accelerated Life Testing.

wick surface temperature, and hence the vapor-gas mixture, is very close to the wall temperature in the gas-blocked region of the condenser. This has been found to be a valid assumptio. from the study of gas controlled pipes [2-5].

In practice, each pipe was divided into 3/4" elements with a thermocouple placed in the center of each interval. The thermocouple temperature readings were input directly into the computer program, which carried out the operations indicated by Eqs. (2-1) and (2-2) and printed out the total number of lb moles of gas in the pipe. Trial calculations have indicated that the discrepancy between using a 0.5" element and a 1.0" element was less than one percent.

2.1.3   Results of Accelerated Testing

Based on previous studies of gas evolution in heat pipes [2-1 through 2-3, 2-6, 2-7], it was assumed that the gas generation rate would be a strong function of tne operating (vapor) temperature. For this reason all heat pipes were tested in a constant temperature chamber. The temperature of the chamber was unaffected by convective air currents in the room and could be held at $\pm 0.5°C$ of the set point.

Initial accelerated life testing was begun with three heat pipes operated at 66°C, 93°C, and 121°C. Other than a small amount of gas which was present from the filling procedure, no detectable additional amount was generated after 39 days of operation. Initial testing was then continued with the temperature increased to 177°C, 204°C and 232°C. Temperature profiles were readily generated at these temperatures over a two week period, the gas evolution rate increasing with increasing temperature.

During initial testing, it was found that burnout occurred at temperatures above 204°C even with the heat pipe in a vertical reflux position. Thus data taken with the heat pipe operated at 232°C was not usable. Calculations of the vapor mass as a function of temperature indicate that burnout above 204°C resulted from liquid depletion. With the heat pipes operating at 177°C and 204°C, the tilt (in the reflux position) was adjusted to the point just above the angle which produced the start of burnout, as evidenced by a rise in the end-cap thermocouple

8

temperature. This procedure was used with all subsequent heat pipes to ensure maximum fluid flow in the wicks.

After completing measurements on the initial set of heat pipes, which determined the temperature range of interest, a set of four heat pipes were operated (in a reflux position) at essentially the same temperature (179.2 - 179.3°C) but at different flow rates (11.0, 12.4, 16.4 and 19.6 watts), to investigate the possibility of a flow rate dependence in the gas generation rate. For a given power, the condenser length was adjusted to achieve the desired temperature. The results are shown in Figure 2-2, where the curves are drawn to a least-squares fit to the data (as with all subsequent graphs). The gas generation data indicates an initial parabolic time dependence, $(time)^{1/2}$, followed by a linear time dependence after the generation of approximately 6×10^{-9} lb moles of gas. Although the power level was varied by nearly a factor of 2, no flow rate dependence was apparent in the data. Thus, any high temperature flow rate dependence must be small, particularly when compared to the temperature dependence.

Having completed the investigation of the flow rate dependence, the program was continued with a study of the time and temperature dependence. Because the initial studies had indicated that the gas evolution rate is very low at low temperatures it was apparent that the investigation of heat pipes at truly reference (normal) operating conditions did not fit within the time frame of this program. Thus all the 8 remaining heat pipes were studied at a series of high (accelerated) temperatures. One of the 179.3°C heat pipes studied for flow rate dependence was included, giving 9 heat pipes at the following series of temperatures: 120.0, 130.0, 140.0, 149.9, 160.0, 170.2, 179.3, 189.7, and 198.2°C. The indicated temperatures are average values of recorded temperatures taken over the entire exposure period at approximately 24 hour intervals. No temperature variations greater than $\pm$ 0.5°C were bserved ove, any significant period of time. Only the three lowest temperature heat pipes could be operated in a heat pipe mode without burnout. The remainder were operated in a reflux position. A 3/4" condenser was exposed in each case giving corresponding flow rates of 7.0, 7.7, 8.9, 10.0, 10.7, 11.4, 12.6, 13.6 and 15.9 watts.
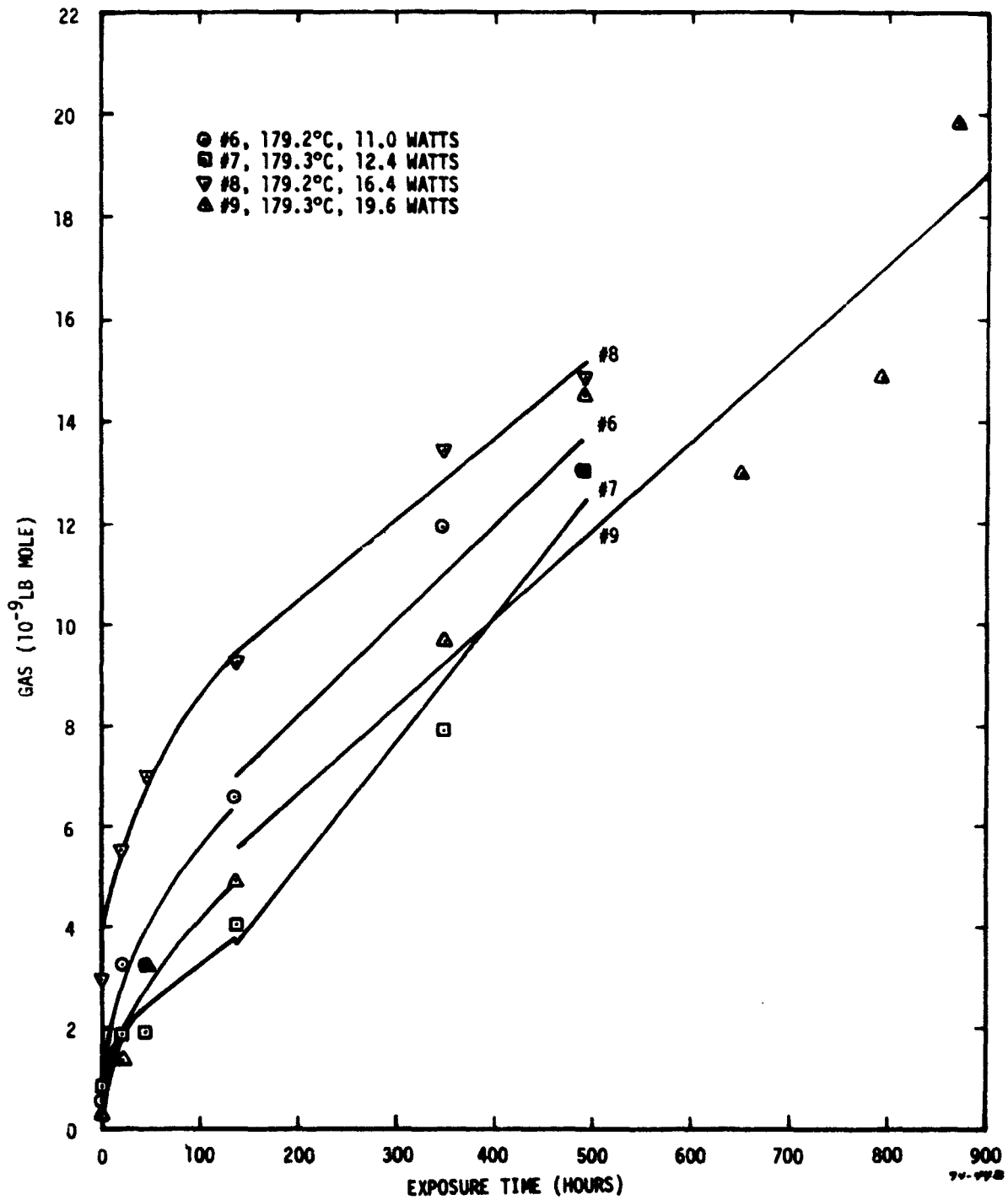
9

FIGURE 2-2. Gas evolution in methanol/stainless-steel heat pipes operated at different power levels to investigate the possibility of a flow rate dependence.

10

The gas generation curves are shown in Figures 2-3 and 2-4. As with the heat pipes studied for flow rate dependence, the gas generation data appears to obey a parabolic time dependence up to approximately 6×10^{-9} lb mole of gas and a linear time dependence beyond this point. Thus, the data points in Figure 2-4 are fitted to a parabolic curve, while the higher temperature data in Figure 2-3 are fitted to a linear time dependence above 6×10^{-9} lb mole and a parabolic dependence below. The data from the 120°C heat pipe is not included because its behavior was significantly different than the other heat pipes. It showed an abnormally high gas generation rate, possibly resulting from a very small leak or from impurities not contained in the other heat pipes.

The scatter in the data appears to be greater for the lower temperature pipes in which only a small amount of gas was generated. This may result from the fact that the results of the computer program are quite sensitive to small variations in the thermocouple readings, particularly for small amounts of gas (10^{-9} lb mole range). Thus the parabolic least squares fits in the range of low gas content were not as good (lower percent of determination) as the linear fits above 6×10^{-9} lb mole.

2.2   Gas Generation Model and Analysis

Stainless steel is reported to undergo uniform corrosion in methanol at a small linear rate (less than 0.1 mpy below 118°C) after long duration exposure [2-8]. No studies of the initial corrosion behavior or of the temperature dependence of the corrosion rate could be found in the literature. In the presence of a catalyst, methanol undergoes dehydrogenation to form formaldehyde gas and hydrogen gas [2-9]:

$$CH_3OH \rightarrow HCHO + H_2 . \tag{2-3}$$

If oxygen is also present, the overall reaction yields formaldehyde and water [2-10]:

$$CH_3OH + 1/2\ O_2 \rightarrow HCHO + H_2O, \tag{2-4}$$
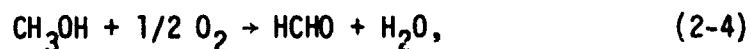
and oxidation of formaldehyde produces formic acid:

$$HCHO + 1/2\ O_2 \rightarrow HCOOH. \tag{2-5}$$

FIGURE 2-3. Gas generation in methanol/stainless-steel heat pipes showing temperature dependence of the gas evolution rate above the parabolic region.

GAS (10^{-9} LB MOLE)

◇ #15, 149.9°C
◉ #13, 140.0°C
▣ #14, 130.0°C
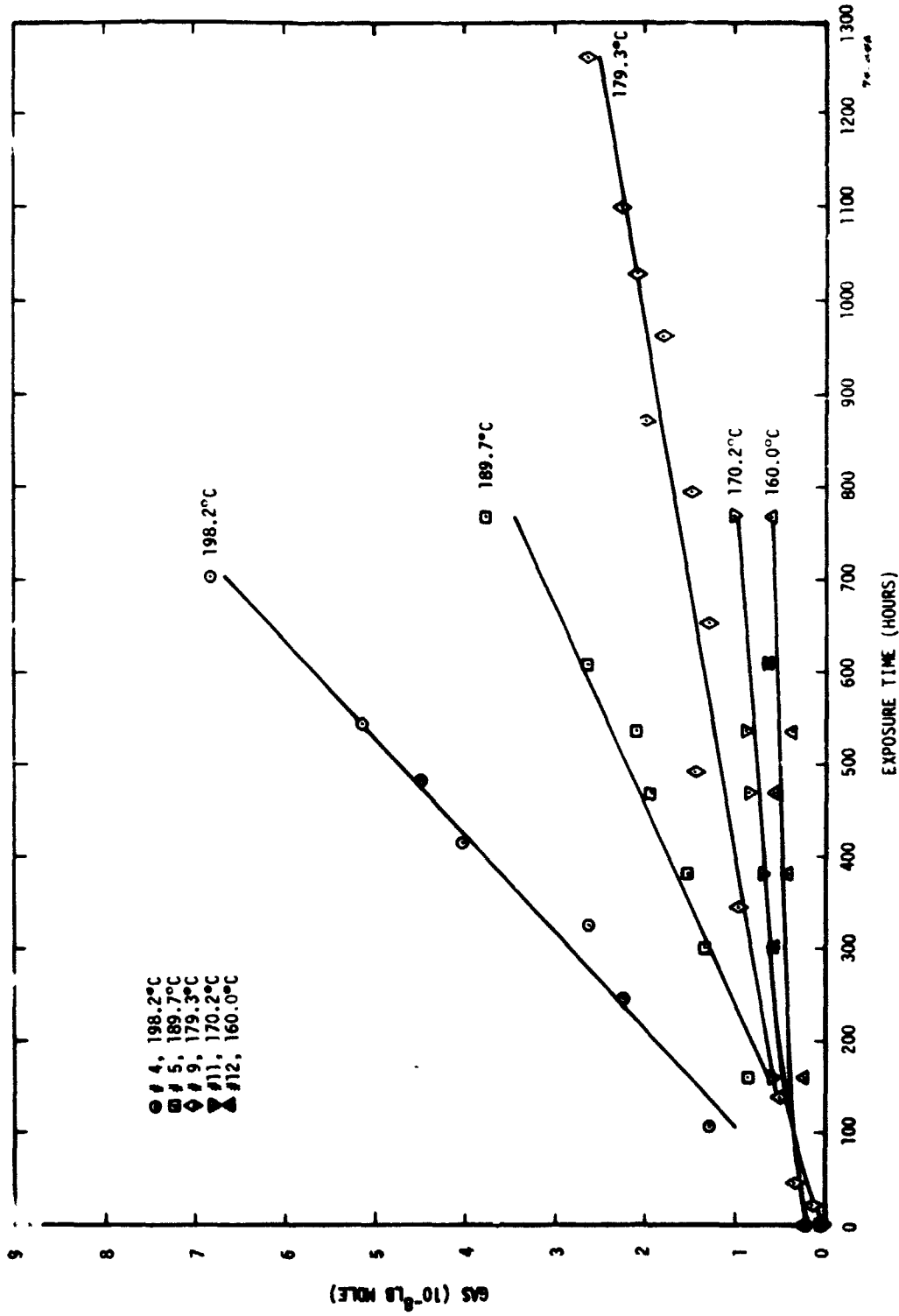
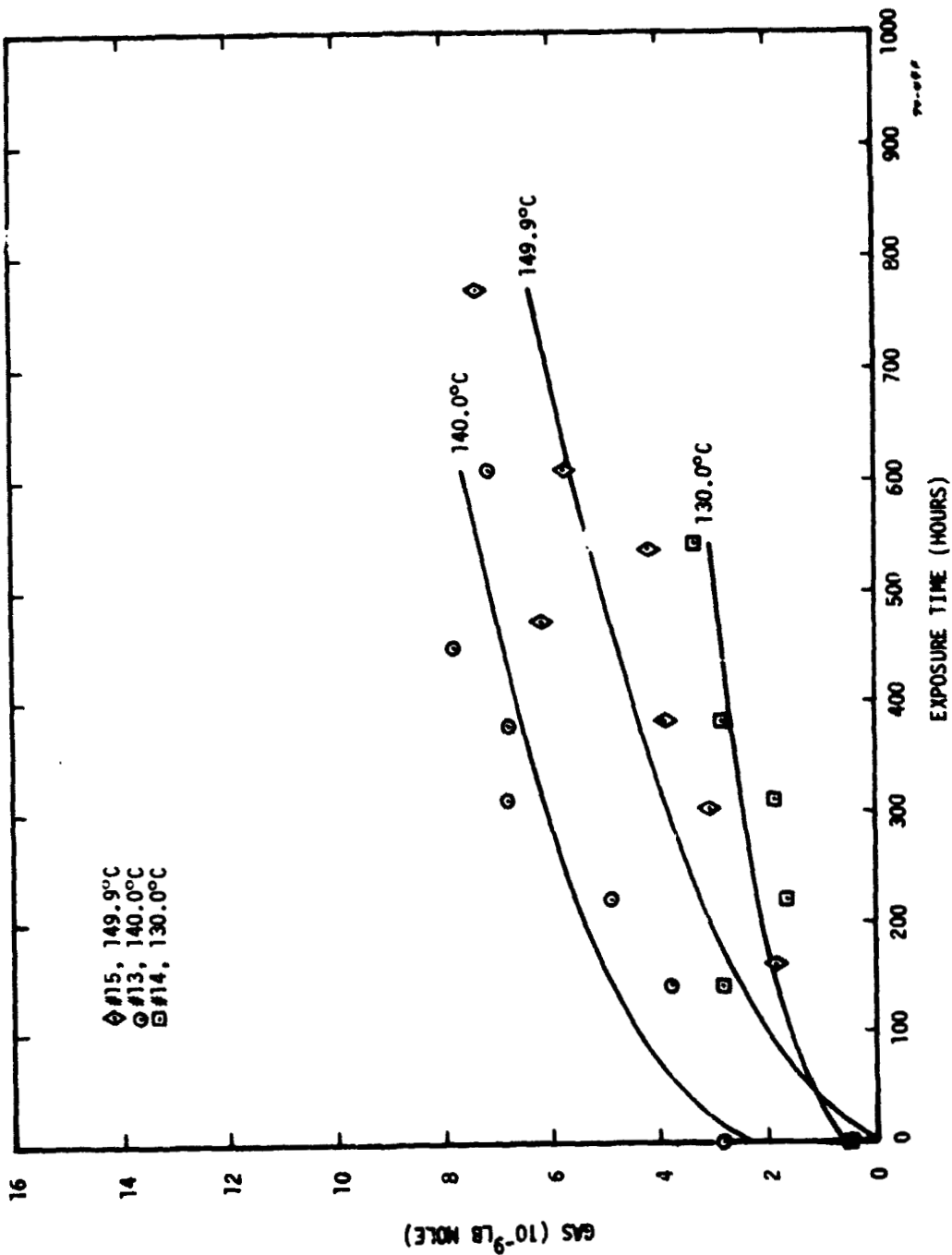0   100   200   300   400   500   600   700   800   900   1000

FIGURE 2-4. Gas generation in methanol/stainless-steel heat pipes showing temperature dependence of gas evolution in the parabolic region.

Methanol/stainless-steel heat pipes might be expected to generate formaldehyde and hydrogen as noncondensable gases, and perhaps formic acid as the reaction proceeds. In fact, an analysis of the gas generated in methanol/stainless-steel heat pipes life tested for 5000 hours between 42-55°C by Kreeb [2-11] showed the presence of formaldehyde plus minor amounts of H_2, CH_4, and CO.

The corrosion rate of stainless steel in formaldehyde is slightly greater (less than 2 mpy at 24°C) [2-12] than in methanol, but the rate increases by more than an order of magnitude in the presence of formic acid (20-50 mpy at 52°C) [2-12]. Uniform corrosion and pitting occur with both of these corrosion reactions [2-8]. Micrographs of sections of methanol/stainless-steel heat pipes life tested at 57°C for 5500 hours by Groll et al. [2-13] showed the presence of a surface film (uniform corrosion) and grain boundary attack. A phenomenological gas generation model is considered below which incorporates corrosion and oxidation theory and contains parameters which may be determined by experiment.

It is assumed that uniform corrosion occurs at all stainless-steel surfaces by the operation of a great number of microscopic galvanic cells [2-14]. The results of this study indicate that passivating film growth with a parabolic time dependence probably occurs initially from the corrosion of the stainless-steel surface in the presence of methanol accompanied by the evolution of a proportional amount of noncondensable gas. Once the passivating film is formed, this corrosion product may then act as a catalyst for reactions (2-3) and (2-4), giving a linear time dependence. Reaction (2-4) may predominate, with the oxygen coming from the small water content of the methanol, based on the results of Keeb [2-11] who found formaldehyde to be the main constituent in the gas. Reaction (2-5) probably plays only a minor role in the corrosion processes.

The transition from the passivating region to the catalytic region should depend on the temperature and the amount of corrosion product present per unit area (effective film thickness) or, equivalently, on the quantity n_c/A, where n_c is the critical gas content and A is the internal corroded surface area. Since the film of corrosion products may be porous and discontinuous, the appropriate area A may be difficult to define. Thus, a critical time $-t_c$ to the transition point can also be defined, as discussed later, which may be a preferable criterion for the transition.

14

Generally accepted theories of film growth during oxidation of metal surfaces assume diffusion through the film of cations away from the metal surface and anions toward the metal surface [2-15, 2-16]. The diffusing ions migrate from one position of minimum potential energy to the next. If Q is the height of the barrier between two potential energy minimums, the probability that an ion will pass over the barrier is proportional to $e^{-Q/kT}$, where Q is called the activation energy, k is Boltzmann's constant, and T is the absolute temperature. This is the temperature dependence found experimentally in solid state diffusion [2-17]. It should be mentioned that the simple interpretation of Q given above is only one of several physical interpretations, which depend on the particulars of film growth theory.

Oxidation theory [2-15] predicts passivating film growth will occur with a parabolic time dependence and an exponential temperature dependence. Assuming a proportional amount of gas is evolved in the process, gas generation in the passivating region, $\frac{n}{A} < \frac{n_c}{A}$, $t < t_c$, should be given by

$$n(t,T) = B_1 \, At^{1/2} e^{-Q_1/kT}, \qquad (2-6)$$

where n is the number of lb moles of gas, t is the time, A is the total internal area of stainless steel in contact with the methanol (166.6 in^2 for these heat pipes), and B_1 is a constant characteristic of the corrosion process. This time dependence has been found to describe hydrogen evolution from steel in boiling water [2-18] but is not common to the (long duration) corrosion of metals generally. Various other forms of time dependencies are also predicted by theory depending on the particular assumptions made [2-19, 2-20]. Over long exposure periods, uniform corrosion with a linear time dependence occurs more commonly.

According to the gas generation model under consideration, after sufficient corrosion product has been produced to act as a catalyst for reactions (2-3) and (2-4), equivalent to a quantity of gas n_c/A lb mole per unit area at the transition point, formaldehyde and hydrogen are produced. These catalytic reactions are considered to predominate beyond the transition point, and would be expected to obey a linear time dependence with a characteristic activation energy Q_2, giving

15

$$n(t,T) = B_2 A t e^{-Q_2/kT}, \qquad (2\text{-}7)$$

for $n/A > \dfrac{n_c}{A}$, $t > t_c$, where B_2 is a constant characteristic of the catalytic reaction. Here Q_2 represents the potential barrier between reacting molecules on the catalytic surface. This temperature dependence is characteristic of many physical and chemical reactions [2-15]. The area A may actually be somewhat larger than geometrical internal area depending on the surface roughness of the stainless steel or corrosion product surfaces.

With dry corrosion the activation energies are generally larger than with wet corrosion, as is apparent from the activation energies shown in Table 2-1. An explanation for this may be that the effective potential barrier is lowered by the electric field across the film created by the local corrosion cell.

The use of this gas generation model in accelerated life testing is that the parameters B and Q can be determined experimentally from data taken under accelerated conditions by plotting $\log \dfrac{\partial n}{\partial t}$ vs. 1/T. Having determined these parameters by measuring the gas evolution at accelerated conditions the gas evolution at any time can be calculated from (2-6) and (2-7) for heat pipes operated under normal conditions. The quantities t_c and n_c/A can be calculated from (2-8) and (2-9), as discussed below.

Least squares fits to the parabolic data are plotted n vs $t^{1/2}$ in Figures 2-5 through 2-7. Plotting $\log \dfrac{\partial n}{\partial t^{1/2}}$ vs $1/T$ results in the curve shown in Figure 2-8, indicating gas generation in the passivating region is described by (2-6), within the accuracy of the data. Calculating the parameters Q_1 and B_1 from the slope and intercept, respectively, results in

$$Q_1 = 6.03 \times 10^{-20} \text{ joules},$$

$$B_1 = 3.66 \times 10^{-8} \text{ lb moles/hr}^{1/2} \text{ in}^2.$$

Table 2-1. Activation energies for corrosion in gaseous and liquid environments.

Material	Environment	Temperature Range (°C)	Activation Energy (10-20 joules)	References
Mild steel	air	below 570	31.3	2 - 21
Stainless steel	oxygen	550-650	20.6	2 - 22
Iron	oxygen	350-450	15.7	2 - 22
Aluminum	oxygen	400-600	25.9	2 - 23
Uranium	air		15.3	2 - 24
Nickel	oxygen	310-345	13.8	2 - 25
Nickel	oxygen	360-440	14.6	2 - 25
Nickel	oxygen	500-1000	24.2	2 - 26
Mild steel	5-20% NaOH	250-355	10.4	2 - 21
Mild steel	10% HCl	40-80	10.1*	2 - 27
18/9 Stainless steel	1N H$_2$SO$_4$	~100	8.63	2 - 28
304 Stainless steel	distilled water	38-149	8.29*	2 - 3
Iron	10% HCl	40-90	3.37*	2 - 27
Lead	10% HCl	40-110	6.81*	2 - 27
Aluminum	70% HNO$_3$	10-120	8.47*	2 - 27
Uranium	water		5-10	2 - 24
Nickel	distilled water	36-81	10.3	2 - 1, 2-2

*Calculated from data contained in referenced papers.
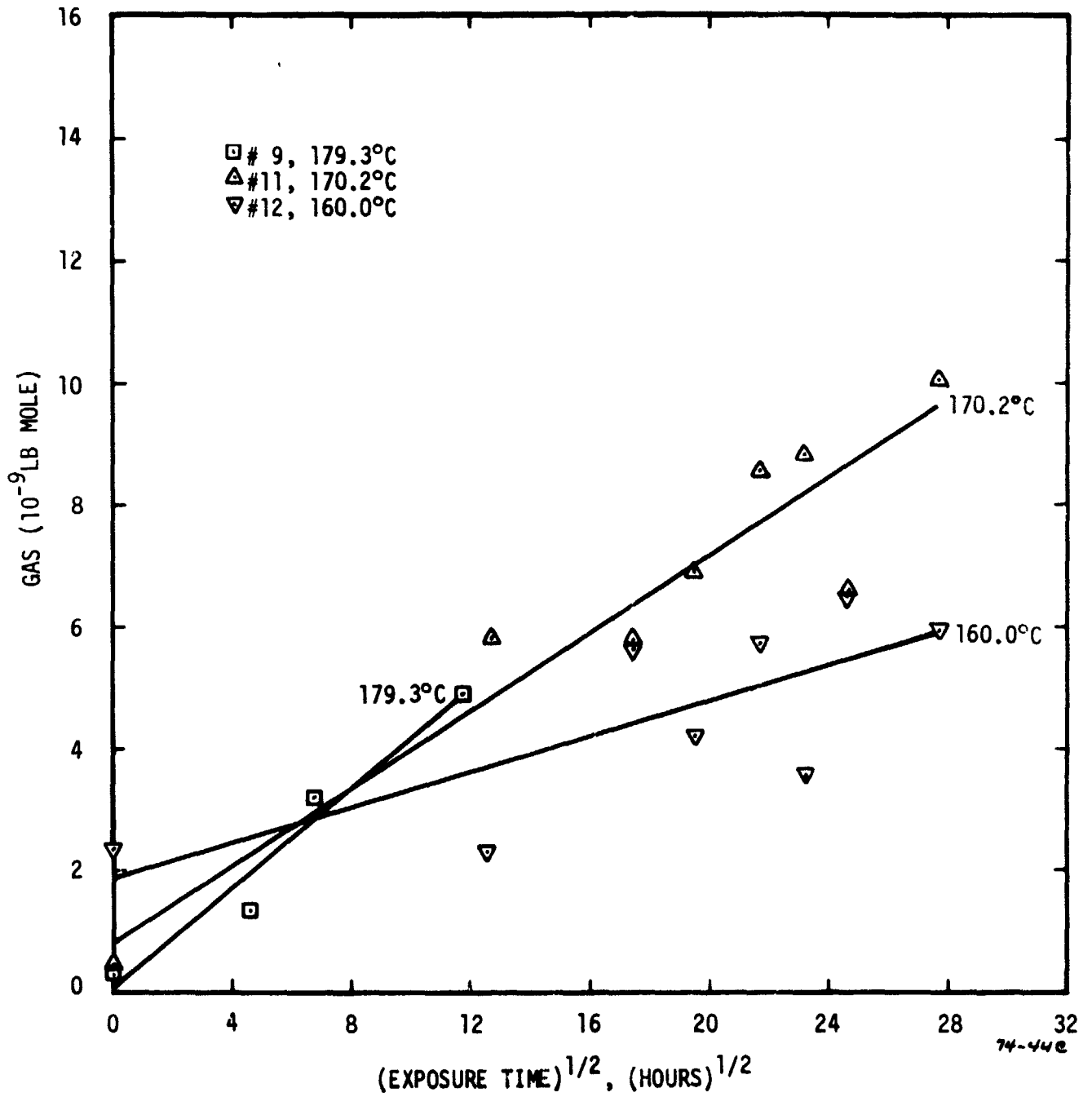
FIGURE 2-5. Gas generation in methanol/stainless-steel heat pipes
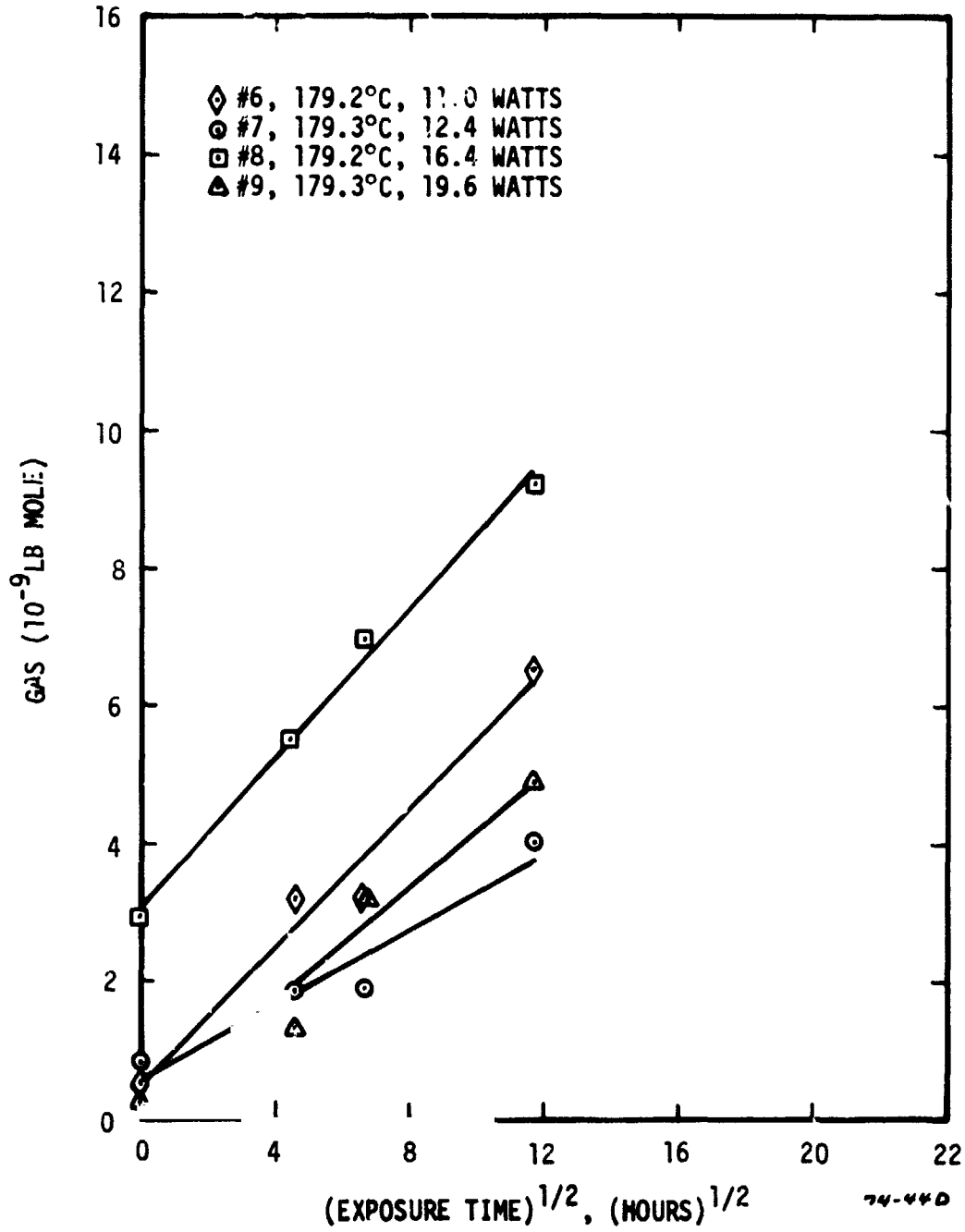showing temperature dependence in parabolic region.

◇ #6, 179.2°C, 11.0 WATTS
⊙ #7, 179.3°C, 12.4 WATTS
⊡ #8, 179.2°C, 16.4 WATTS
△ #9, 179.3°C, 19.6 WATTS

GAS (10^{-9} LB MOLE)

(EXPOSURE TIME)$^{1/2}$, (HOURS)$^{1/2}$

74-440

FIGURE 2-6. Gas generation in methanol/stainless-steel heat pipes in parabolic region.
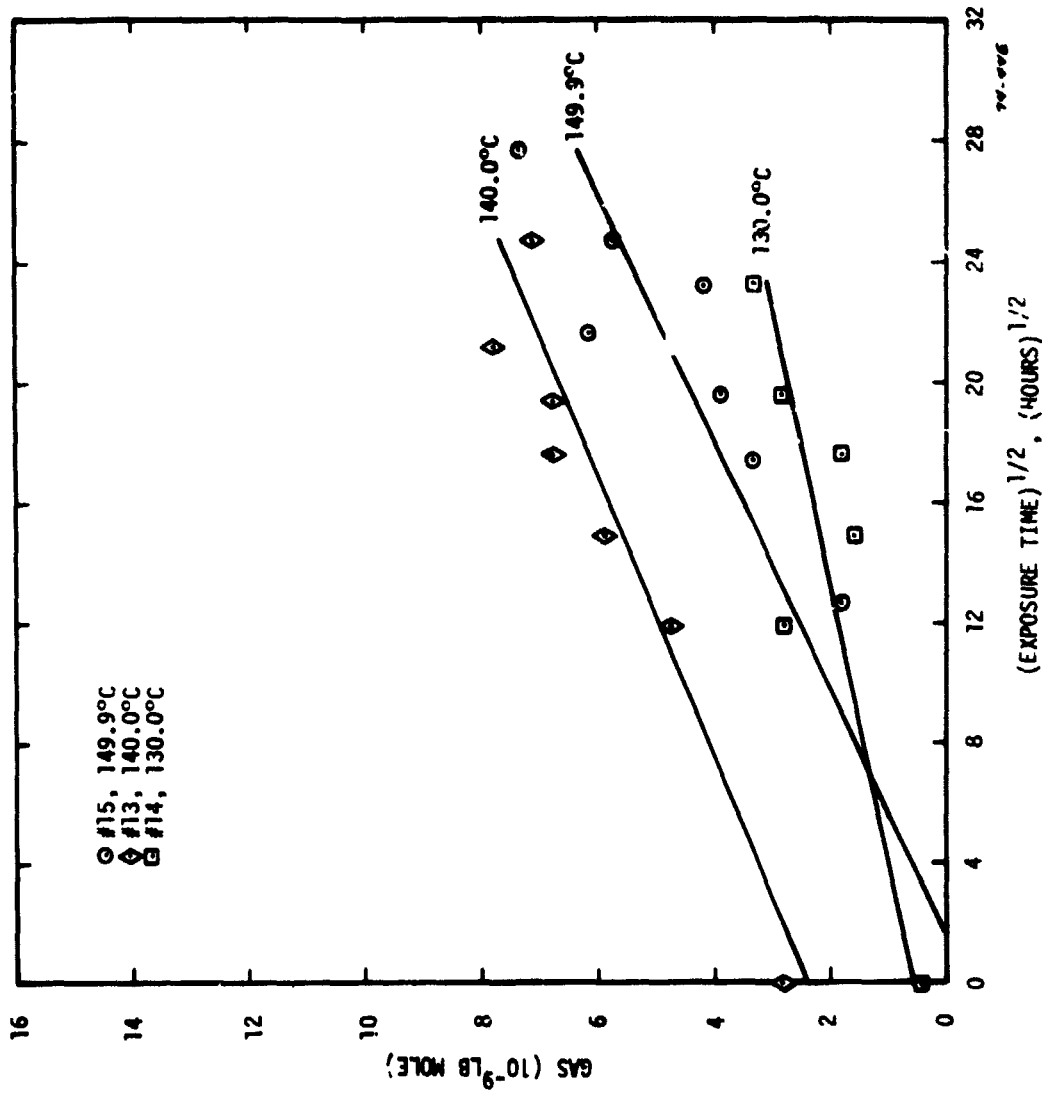
19

FIGURE 2-7. Gas generation in methanol/stainless-steel heat pipes showing temperature dependence in the parabolic region.
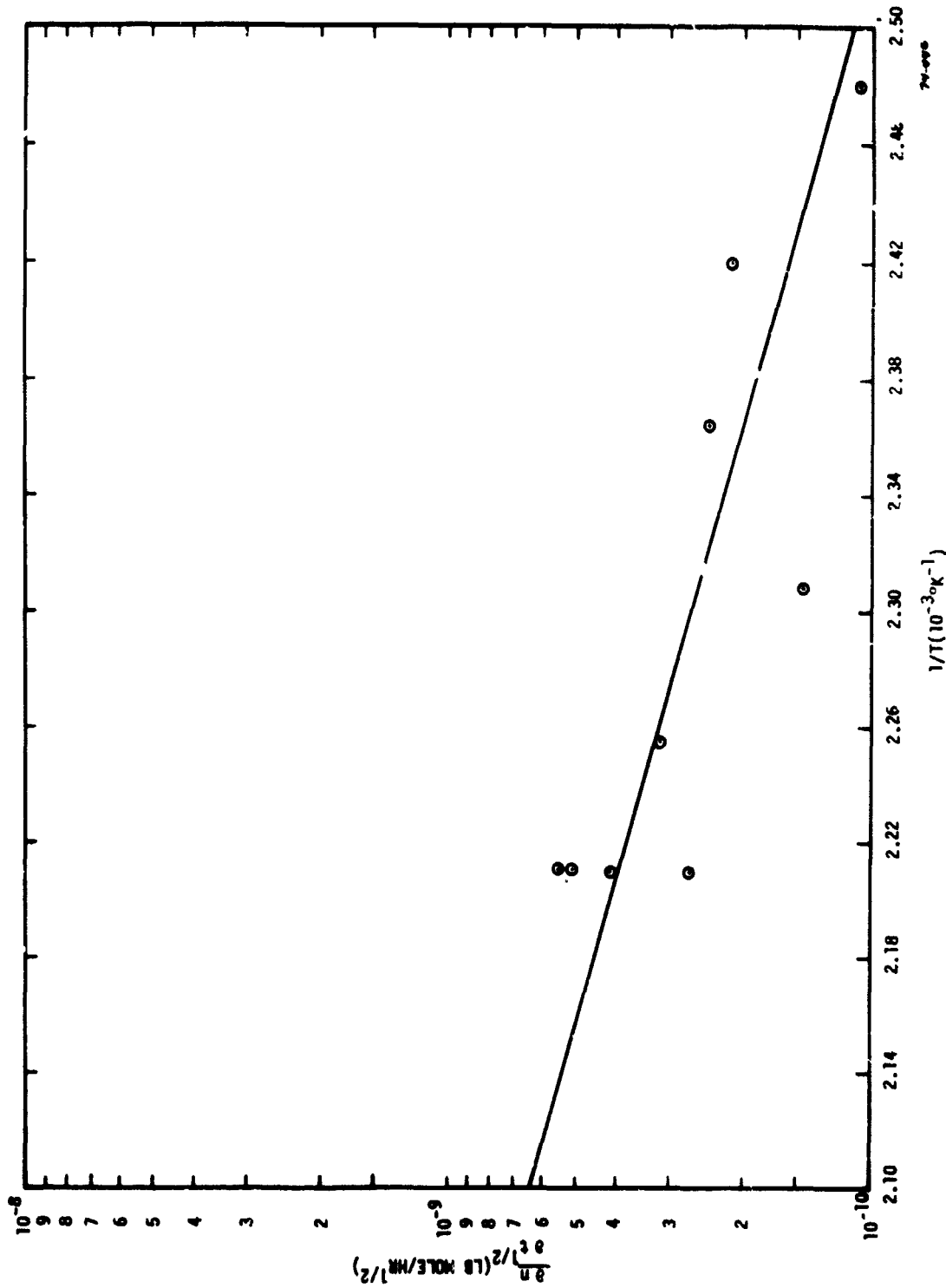
FIGURE 2-8. Accelerated testing data of methanol/stainless-steel heat pipes in the parabolic region, $\log \frac{\partial n}{\partial t}^{1/2}$ vs $1/T$.
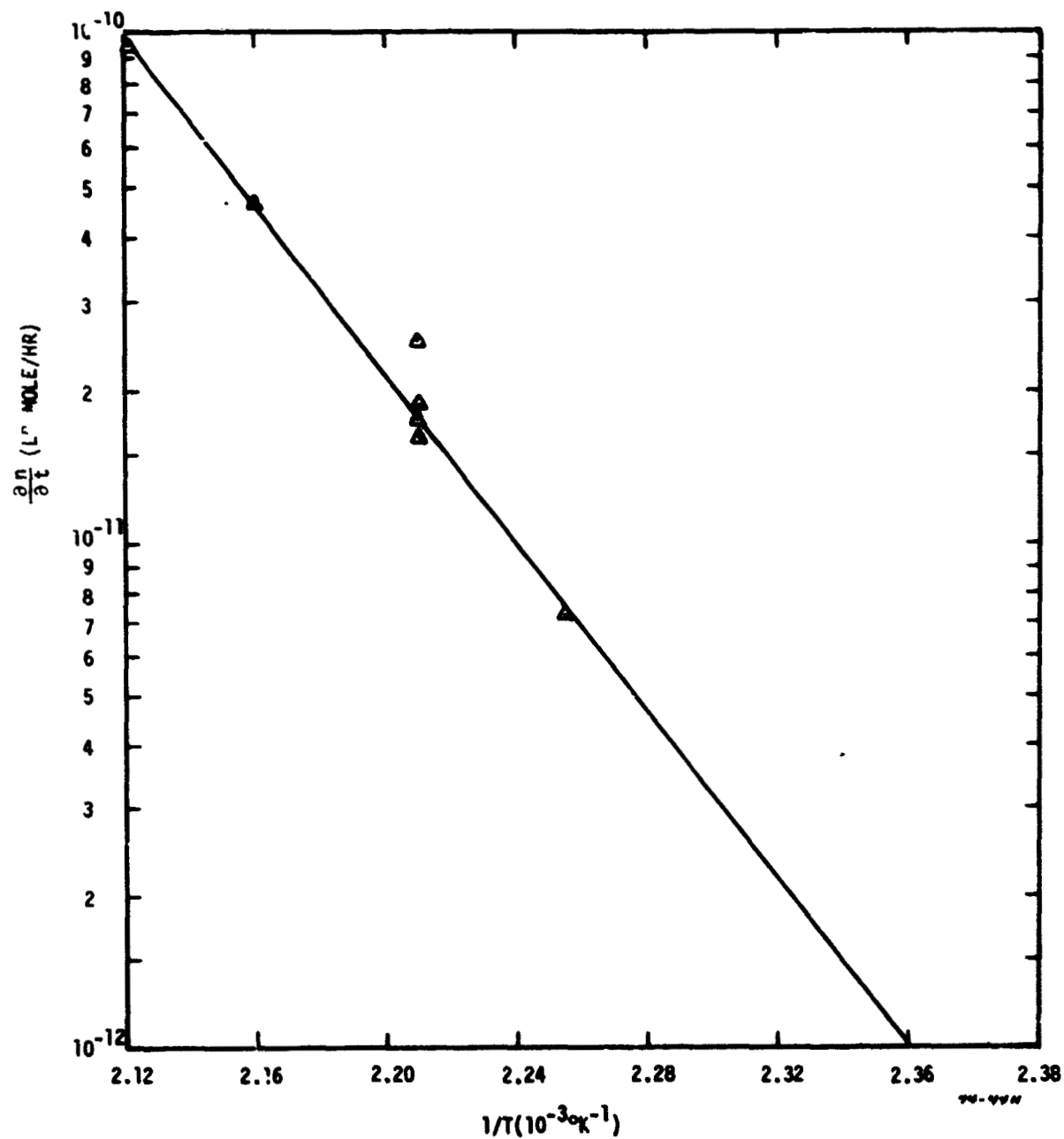
FIGURE 2-9. Accelerated testing data of methanol/stainless-steel heat pipes in the linear region, $\log \frac{\partial n}{\partial t}$ vs 1/T.

A plot of $\log \frac{\partial n}{\partial t}$ vs $^1/T$ in the linear region results in the curve shown in Figure 2-9, showing good agreement with (2-7). Calculating the parameters for the gas generation behavior beyond the passivating region results in

$$Q_2 = 26.7 \times 10^{-20} \text{ joules,}$$

$$B_2 = 3.79 \times 10^5 \text{ lb mole/hr in}^2.$$

The transition point t_c between the passivating and catalytic regions may be defined as the point beyond which catalytic reactions predominate, i.e., the time at which the gas generation rates, $\frac{\partial n}{\partial t}$, are equal. Equating the slopes, $\frac{\partial n}{\partial t}$, of Eqs. (2-6) and (2-7) results in:

$$t_c = \frac{B_1^2}{4B_2^2} \exp \left[\frac{2(Q_2 - Q_1)}{kT} \right] \qquad (2\text{-}8)$$

for the critical time. The critical gas content per unit area (equivalent to a critical film thickness of corrosion products in this model) is found by substituting Eq. (2-8) into Eq. (2-6):

$$\frac{n_c}{A} = \frac{B_1^2}{2B_2} \exp \left[\frac{Q_2 - 2Q_1}{kT} \right] \qquad (2\text{-}9)$$

Thus, as the temperature increases, both t_c and n_c/A decrease. This is reasonable since less catalytic material would be required to obtain a given gas generation rate as the temperature increases. The value of $n_c \sim 6 \times 10^{-9}$ 16-mole ($n_c/A \sim 3.6 \times 10^{-11}$ lb-mole/in^2) which was observed as the approximate value of the critical gas content in the temperature range 160-179°C agrees reasonably well with Eq. (2-9). At 170°C, Eq. (2-9) yields $n_c/A = 4.3 \times 10^{-11}$ lb-mole/in^2.

2.3   Conclusions and Recommendations:

The behavior of the gas evolution in methanol/stainless-steel heat pipes was found to depend on the amount of gas per unit area generated during accelerated testing. Below a critical value n_c/A given by Eq. (2-9), or critical time t_c given by Eq. (2-8), the time dependence is explained best by a parabolic function, indicative of the growth of a passivating film of corrosion products. The data in this region can be correlated with a model of film growth resulting in Eq. (2-6), which contains parameters to be determined by experiment. Above the critical point given by Eqs. (2-8) and (2-9), a linear time dependence was observed. In this region the data can be correlated with a model of catalytic decomposition of methanol to formaldehyde and hydrogen on the surface of the corrosion products, resulting in Eq. (2-7). No flow rate dependence was found within the accuracy of the data. In application to other types of methanol/stainless-steel heat pipes, the gas generation may vary depending on the type of stainless steel, the purity of the methanol, and other factors; but it is expected that the behavior could be explained by the same form of the Eqs. (2-6) and (2-7), with associated critical values (2-8) and (2-9), only the value of the parameters may change.

Based on the results of this and the previous study [2-1] it appears that this method of accelerated life testings has a broad applicability to heat pipe systems, even when not a great deal is known concerning the actual gas evolution mechanisms. This method of accelerated life testing can now be applied to other important types of heat pipes with good probability of success.
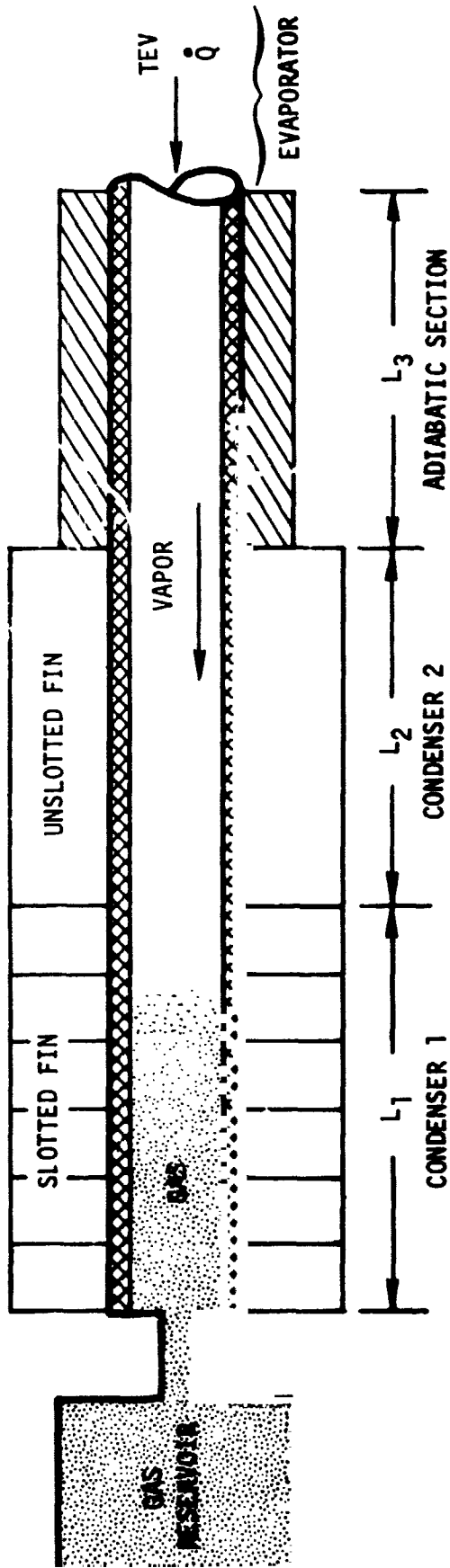
3.0   GASPIPE EXTENSIONS

The TRW GASPIPE computer program, which was developed on the present contract and documented in **Ref.** [3-1], "User's Manual for the TRW Gaspipe Program", has been extended to include two condenser sections. Since the new version of the program is described in detail in the revised user's manual, (**Ref.** [3-2]), it will suffice here to summarize the programs capabilities.

The motivation for extending the original GASPIPE program is the frequent design of heat pipes with a second condenser section having as low an axial conductivity and effective sink temperature as possible. Such sections are used adjacent to the gas-reservoir entrance to minimize the partial pressure of the reservoir vapor, thus allowing smaller reservoirs and/or a tighter control band. In the case of a wicked cold-reservoir design, the low-conductivity section minimizes heating of the reservoir by axial conduction from the active portion of the condenser. In the case of a non-wicked hot-reservoir design, wherein the partial pressure of the reservoir vapor is set by the temperature of the nearest portion of saturated wick, the low-conductivity section minimizes warming of this portion.

The original GASPIPE program cannot treat such situations if the sink temperatures of the two condensers are unequal and the gas front develops in the condenser farthest from the reservoir. In addition, the original program is limited to either two condensers or one condenser and one adiabatic section, and many applications require two condensers and an adiabatic section. The extension of the program remedies these deficiencies.

The situation to which the revised program, GASPIPE 2, is applicable is depicted schematically in Figure 3-1. In this figure, the axial conductivity of condenser 1 is minimized by the use of slotted fins. All parameters including the sink temperature that describe condenser 1, can be set differently from those describing condenser 2. Thus the fins attached to condenser 1 may have a special coating to achieve a low effective sink temperature, or the heat-pipe wall itself may be thinner or even be a different material to achieve a low axial conductivity. A typical condenser cross-section is shown in Figure 3-2. The program is not limited to the geometry shown, non-circular and non-axisymmetric configurations can also be studied.

a. Schematic Diagram of a Gas-Loaded Heat Pipe
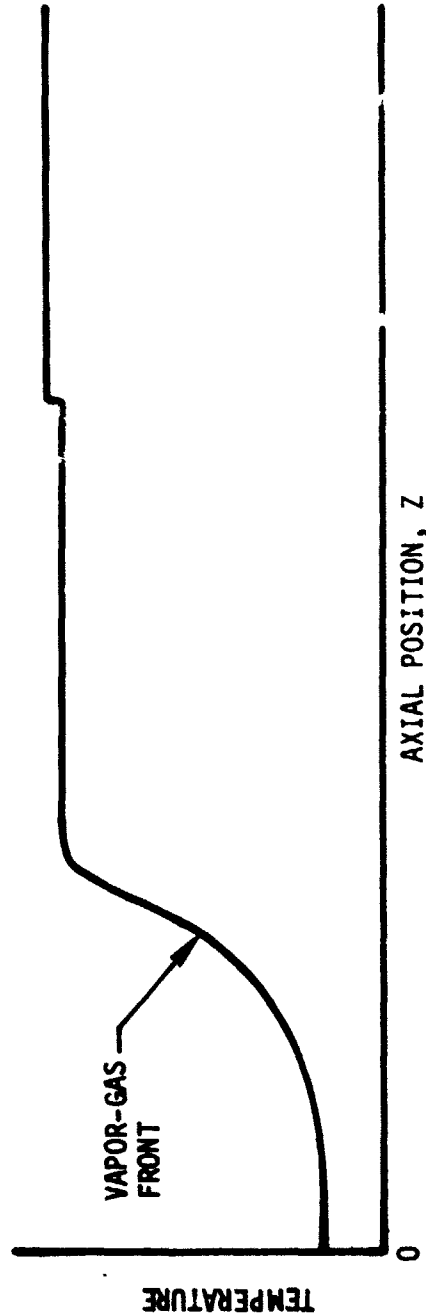
b. Temperature Distribution

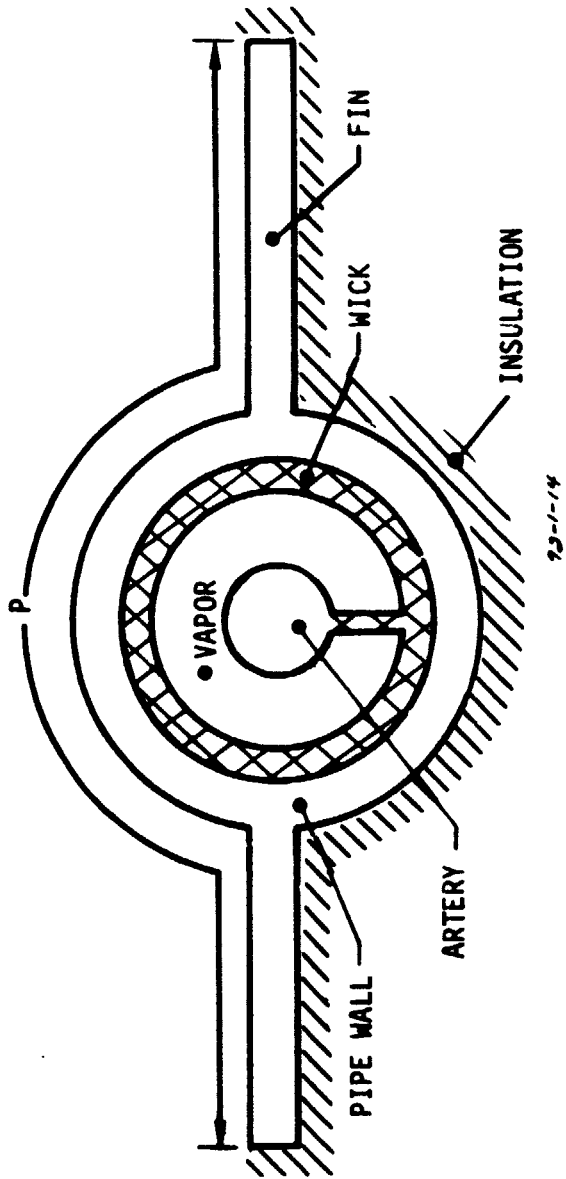FIGURE 3-1. Vapor-Gas Front Analytical Model for a Gas-Loaded Heat Pipe.

FIGURE 3-2. Cross-section of Condenser

In addition to the extensions, the new GASPIPE 2 program retains all the capabilities of the original GASPIPE program, which allow one to:

o   Calculate the wall-temperature profile along a gas
    loaded heat pipe.

o   Calculate the amount of gas loading necessary to
    obtain a desired evaporator temperature at a
    desired heat load.

o   Calculate the heat load versus the evaporator
    temperature for a fixed amount of gas in the pipe.

o   Calculate the heat and mass transfer along the
    pipe, including the vapor-gas front region.

o   Calculate the heat leak when the condenser is
    filled with gas.

o   Calculate whether or not freezing occurs in the
    condenser and, if so, at what rate.

o   Determine the information required to size the gas
    reservoir of gas-controlled heat pipes.

The program contains numerous reservoir options that allow it to be used for hot or cold passive-control as well as heated-reservoir active-control heat pipes.

GASPIPE 2 is based on a one-dimensional steady-state analysis that results in two simultaneous first-order ordinary differential equations that govern (i) the mole fraction of the noncondensable gas and (ii) the vapor velocity. These are integrated with the forth-order Runge-Kutta routine. The addition of the second condenser section with a different sink temperature required extensive modification to the original program. Previously, a single solution curve was obtained by numerical integration that could be translated within the condenser until a position corresponding to the required heat flow or the required inventory was achieved. With a step change in condenser properties that occurs with two condensers, translation is no longer possible. An initial solution is obtained for the case of complete gas blockage of the heat pipes by first integrating once backward from the adiabatic section with properties

of condenser 2 and then repeatedly forward with properties of condenser 1 until proper conditions are met at the intersection of the two curves. The two curves are then translated until their intersection coincides with the boundary between condensers 1 and 2. With the initial gas-blocked profile as a base, a solution curve for a non-gas-blocked region is obtained by selecting a point along the gas-blocked curve, slightly perturbing the value of the solution at that point, and then integrating toward the evaporator. The solution curve thus generated automatically seeks a condition of no gas blockage. Solutions are repeatedly obtained in this way, but with different starting points along the gas-blocked curve, until either the calculated amount of noncondensable gas or the total heat rejected agrees with the specified amount. In some cases, the correct solution is obtained by repeated integrations from the beginning condenser 1 with suitable adjustments of the initial conditions. For details of the program, refer to the user's manual already cited.

4.0 PRIMING STUDIES

Many heat-pipe applications require both the high performance
of an arterial design and the variable-conductance characteristics obtained
through the use of noncondensable gas. The presence of gas, however, can
interfere with the priming and operation of arteries. Part of our research
task was to study arterial performance in the presence of gas.

During arterial priming, noncondensable gas can result in
bubble entrapment. At TRW, we have developed an approach to vent gas
through holes in a foil-walled section of the artery at the evaporator end.
Our research task calls for detailed study of this new solution of arterial
priming with a glass heat pipe. As will be described presently, such an
apparatus was fabricated that closely approximates actual heat-pipe
configurations currently in use.

Noncondensable gas also causes problems in the operation of
arterial heat pipes with ammonia. Pressure fluctuations which only appear
when there is some condenser blockage by noncondensable gas, result in
depriming of arteries. Our research task also calls for both a theoret-
ical and experimental investigation of the mechanism of these fluctuations.

4.1 Theoretical Study of Pressure Fluctuations in a Gas-Controlled Ammonia Heat Pipe

Pressure fluctuations in gas-controlled ammonia heat pipes
were first reported by Edelstein, Roukis and Loose (Ref. [4-1]). They
observed 0.12 to 0.14 psi irregular fluctuations with a period ranging
between 0.25 and 0.50 minutes in an ammonia heat pipe containing nitrogen
gas for control of the active condenser length. The pipe was approximately
one inch in diameter with a 46 inch long evaporator and an equally long
condenser. The magnitude of the fluctuations increased somewhat with
heat load, but was independent of tilt. Their magnitude was sufficient
to deprime the tunnel artery, which was the basis for their high perform-
ance (150,000 watt-inch) heat pipe. With no control gas present, they
reported a marked decrease in amplitude and "number" (frequency?) of

oscillations so that the pipe performed as desired.

Similar problems with the priming of a high-perfomance ammonia heat pipe were encountered by TRW (Ref. [4-2]). A pressure transducer was installed and indicated excessive pressure fluctuations. In this case the fluctuations, while still rather irregular, were much more nearly periodic in nature with a period of approximately 1.1 to 1.2 minutes and an amplitude of approximately 0.31 lb_f/in^2 at low heat load. Data were obtained with and without additional mass added to the evaporator as follows:

Mass of Aluminum on Evaporator lb_m	Control Gas	Steady Power Watts	Pressure-Fluctuation Amplitude lb_f/in^2
0	None	100	< 0.02
	Argon	100	~ 0.07
	"	3	~ 0.45
3.5	"	100	< 0.07
	"	6	< 0.33
28.0	"	100	< 0.15
	"	3	< 0.010

Contrary to the experience reported by Edelstein, the most severe oscillations occurred at low heat loads. However, in these tests the condenser sink was massive, and the severe oscillations occurred when, at low heat loads, the gas front penetrated into the adiabatic section whose mass was only that of a 0.50-inch outside diameter tube with 0.028-inch thickness and the diametral wick.

4.1.1 Possible Oscillation Mechanisms

The long period of the oscillations, 15 to 70 seconds, strongly suggests a mechanism limited by heat or mass-diffusion rates. The possibility of gravity waves playing a part, for example, may be ruled out by considering the time scale for such a mechanism

$$t_{gravity} \approx \sqrt{\frac{\rho D}{\Delta \rho g}} \pm 0.1 \text{ Sec.}$$

30

where ρ is the density of the gas, D is the pipe diameter, and g is the gravitational acceleration. Such considerations would rule out with even greater force acoustic-resonance phenomena whose period would be on the order of the pipe length divided by the acoustic velocity. In comparison, consider typical characteristic times for diffusion phenomena shown in Table 4-1. We will see presently that the theoretical period of the oscillation is of the same order of magnitude (within a factor of 4) as a characteristic delay time. Therefore, the times most in agreement with the experimental ovservations are those for phenomena 1, 2, 3 and 5 in Table 4-1.

TABLE 4-1
CHARACTERISTIC TIMES FOR
DIFFUSION PHENOMENA

PHENOMENON	FORMULA FOR CHARACTERISTIC TIME	NUMERICAL VALUE OF CHARACTERISTIC TIME
1. Mass diffusion in the gas phase through one inside diameter	$\dfrac{(\text{pipe diameter})^2}{(\text{diffusion coef.})}$	10 Sec.
2. Mass diffusion in the gas phase through the gas front	$\dfrac{(\text{gas-front length})^2}{(\text{diffusion coef.})}$	100 Sec.
3. Mass diffusion in the liquid phase through the wick thickness	$\dfrac{(\text{wick thickness})^2}{(\text{diffusion coef.})}$	50 Sec.
4. Heat diffusion in the liquid phase through groove depth	$\dfrac{(\text{groove depth})^2}{(\text{thermal diffusivity})}$	0.1 Sec.
5. Heat diffusion in the liquid phase through the diametral wick half thickness	$\dfrac{(\text{wick thickness})^2}{(\text{thermal diffusivity})}$	10 Sec.

Three possible disturbances can be conceived on the basis of this table:

A. A disturbance based upon the time lag between a convective distortion of the gas front and its re-establishment by diffusion.

B. A disturbance based upon a convective distortion of the gas front and the consequent effect upon dissolved gas in the condensate which in turn triggers nucleation in the evaporator.

C. A disturbance based upon the time lag between the filling of a void in the diametral wick with liquid and the formation of a bubble by boiling in the wick where it contacts the wall.

These three correspond with Items (1 or 2), (3), and (5) respectively in Table 4-1. Item (4), which corresponds to periodic bo boiling in the grooves, is seen to have too fast a characteristic time.

Further consideration of the time necessary for the liquid to flow from condenser to evaporator would seem to eliminate disturbance B above. Further, while a diametral wick was used in the TRW experiments, a spiral artery was used in work of Ref.[4-1]. The feed wicks of that pipe do not seem to have a configuration favoring boiling within them, thus disturbance C seems unlikely. Disturbance A above is thought most likely, and we now consider a simplified model of it.

4.1.2   A Simplified Model

In a heat pipe a pressure change dP is caused by (or accompanied by) a temperature change dT given by the Clausius-Clapeyron relation,

$$\frac{dP}{P} = \frac{h_{fg}M}{\Re T} \frac{dT}{T} \quad ,$$

(4-1)

where h_{fg} and M respectively are the latent heat and molecular weight of the working fluid, and $\mathscr{R}$ is the universal gas constant. The observed fluctuations in dP/P are on the order of 10^{-3}; hence, the fluctuation in dT/T is on the order of 10^{-4}. The pressure and temperature fluctuation are also accompanied by a prompt movement dz of the gas front. If A_c is the cross-sectional vapor area of the condenser, and V is the total gas-blocked volume that contains N moles of vapor and gas at temperature T_s, then

$$dz \ A_c \ = \ -dV \ = -d(\frac{N\mathscr{R}T_s}{P}) = V \ \frac{dP}{P} \ ,$$

or, using (4-1), we write

$$dz = \frac{V}{A_c} \ \frac{h_{fg}M}{\mathscr{R}T_s} \ \frac{dT}{T} \ . \tag{4-2}$$

The movement of the gas front by dz opens up new heat-transfer area so that the heat-transfer rate $\dot{Q}$ lost in the condenser goes up by dQ_1:

$$dQ_1 = UPdz \ (T - T_s), \tag{4-3}$$

or, using (2), we write

$$dQ_1 = UP \ (T-T_s) \ \frac{V}{A_c} \ \frac{h_{fg}M}{\mathscr{R}T_s} \ \frac{dT}{T} \ . \tag{4-3}$$

Here, U is the heat-transfer coefficient and P is the condenser perimeter. There is also a slightly augmented heat transfer due to the increase in $T - T_s$,

$$dQ_2 = UPz \ dT \tag{4-4}$$

where z is the active condenser length. We imagine that the latter is prompt in terms of a few seconds while the former may be delayed by a time τ of some tens of seconds or a minute due to the slowness with which the gas diffuses out of the way of the condensing vapors.

The heat loss from the condenser in time dT is $dQ_c = dQ_1 + dQ_2$, where we can write $\dot{Q}_c$ as

$$\dot{Q}_c = (T - T_s) \frac{1}{R_0} \left[1 + \frac{1}{R_0} \frac{dR_0}{dT} (T(t-\tau) - T_0) \right]. \qquad (4-5)$$

Here, T_0 is the mean vapor temperature, and from Eqs. (4-2), (4-3) and (4-4), we have (to first order in $T - T_0$)

$$R_0 = \frac{1}{UPz_0}, \qquad (4-6)$$

and

$$\frac{1}{R_0} \frac{dR}{dT} = \left(\frac{V}{A_c z_0} \right) \left(\frac{h_{fg}M}{\mathcal{R}T_s} \right) \left(\frac{1}{T_0} \right). \qquad (4-7)$$

In order for the evaporator temperature T to rise by dT a quantity of heat dQ_{eac} is promptly needed to heat the evaporator, adiabatic, and condenser masses:

$$dQ_{eac} = [m_e c_e + m_a c_a + m_c(z/L_c)c_c]dT$$

where m and c are the mass and specific heat of the evaporator, adiabatic or condenser sections, which are distinguished by the subscripts $(\ )_e$, $(\ )_a$ and $(\ )_c$ respectively, and L_c is the total condenser length. There is also a delayed need of heat dQ_z needed to warm the segment of condenser brought into service:

$$dQ_z = (m_c/L_c)c_c(T - T_s)\, dz,$$

or, using (4-2),

$$dQ_z = (m_c/L_c)c_c(T - T_s) \frac{V}{A_c} \frac{h_{fg}M}{\mathcal{R}T_s} \frac{dT}{T}.$$

The steady electrical heating of the evaporator goes into supplying this heat as well as the heat losses [Eq. (4-5)] during a temperature fluctuation], that is

$$\dot{Q}dt = [m_c c_e + m_a c_a + m_c(z/L_c)c_c] \frac{dT}{dt}\Big|_t dt$$

$$+ (m_c/L_c)c_c \frac{(T - T_s)}{T_0} \frac{V}{A_c} \frac{h_{fg}M}{\mathcal{R}T} \frac{1}{T} \frac{dT}{dt}\Big|_{t-\tau}dt +$$

34

$$+ (T - T_s) \frac{1}{R_0} [1 + \frac{1}{R_0} \frac{dR_0}{dT} (T(t - \tau) - T_0)]dt .$$

Denote

$$\tau_p = R_0 [m_e c_e + m_a c_a + m_c(z_0/L_c)c_c], \qquad (4\text{-}8)$$

$$\tau_d = R_0 [(m_c/L_c)c_c (\frac{T_0 - T_s}{T_0}) \frac{V}{A_c} \frac{h_{fg}M}{\mathcal{R}T_s}], \qquad (4\text{-}9)$$

$$T_c = T_s + R_0 \dot{Q}, \qquad (4\text{-}10)$$

$$B = (T_0 - T_s) \frac{1}{R_0} \frac{dR_0}{dT} \bigg|_{T - T_0}, \qquad 4\text{-}11)$$

$$T' = T - T_0, \qquad (4\text{-}12)$$

The heat balance equation becomes

$$0 = \tau_p \frac{dT'}{dt} \bigg|_t + \tau_d \frac{dT'}{dt} \bigg|_{t - \tau} + T'(t) + BT'(t - \tau)$$

$$+ B \frac{T'(t)\, T'(t - \tau)}{T_0 - T_s} . \qquad (4\text{-}13)$$

Eq. (4-13) is a differential-difference equation which are discussed in Refs. [4-3] and [4-4]. It embodies a prompt effect of the thermal capacities of the evaporator adiabatic and condenser sections in resisting temperature change (the first term), a delayed effect of the thermal capacity of the condenser exposed when the front moves (the second term), a prompt effect of increased heat losses in the working portion of the condenser when the vapor temperature rises (the third term), a delayed effect of increased heat loss due to movement of the front in exposing more condenser surface (the fourth and fifth terms). This last factor is represented by the first-order linear term $BT'(t - \tau)$ representing exposure of new condenser surface to the old vapor temperature T_0 and a second-order, nonlinear term $[B/(T_0 - T_s)] T(t) T'(t - \tau)$ representing the increased heat transfer from new surface due to the rise T' in vapor temperature above T_0. This latter is clearly small and will be neglected when the equation is examined for what it says about the period of the disturbance.

In order to say anything about the __amplitude__ of the disturbance,
it is necessary to retain nonlinear terms. That the only nonlinear
term shown in Eq. (4-13) is the dominant one is not clear. In the course
of deriving Eq. (4-13) many inherently nonlinear terms were neglected;
for example, the change in gas volume V due to movement of the front or
to the change in temperature T (taken to be T_0) in the equations for
the B and τ_d terms [Eqs. (4-7) and (4-11) and (4-9)]. Since the factor
of concern is V/T and V decreases upon increase in T, the two effects
are additive rather than self-cancelling. Furthermore, in the tests of
Ref. (4-1), spray cooling was used, and radiation is often an important
heat-transfer mechanism in rejecting heat from the condenser in actual
applications. Where either evaporation (spray cooling) or boiling or
radiation acts at the condenser, an increase in $T - T_s$ gives more than
a proportional increase in the heat rejected, and hence another source
of nonlinearity arises. A mitigating factor in favor of retaining the
nonlinear term of (4-13) for an amplitude analysis is that it has much
the same form of a "stiffening term" of a spring-mass system.

4.1.3   Analysis of the Equation

Much information can be obtained from Eq. (4-13) if we simplify
it by neglecting the nonlinear term and considering the special case
$\tau_d = 0$. In this case, we have

$$\tau_p \frac{dT'}{dt}\bigg|_t + T'(t) + B\,T'(t-\tau) = 0 . \qquad (4-14)$$

We seek a solution of the form

$$T' = A\,e^{\zeta t}, \qquad (4-15)$$

where $\zeta = \alpha + i\omega$.

If α is positive, our linearized theory predicts that the solution will
become infinite. Actually, the fluctuations will be limited by nonlinearities
or other small effects that we have neglected. If α is negative, the
solution is damped and we do not expect fluctuations.

The characteristic equation is obtained by substituting Eq. (4-15) into (4-14):

$$\tau_p \zeta + 1 + b \ e^{-\zeta\tau} = 0, \tag{4-16}$$

or in terms of its real and imaginary parts,

$$\tau_p \alpha + 1 + B \ e^{-\alpha\tau} \cos \omega\tau = 0, \tag{4-17}$$

$$\omega \tau_p - B \ e^{-\alpha\tau} \sin \omega\tau = 0 \tag{4-18}$$

We first ask if there are any non-oscillatory solutions ($\omega = 0$) that are unstable ($\alpha > 0$). By setting $\omega = 0$ in (4-17), we obtain

$$\alpha = -1 - B \ e^{-\alpha\tau}. \tag{4-19}$$

Since $B > 0$, we deduce that if the solution is non-oscillatory, then it is stable.

We now look for an unstable ($\alpha > 0$) oscillatory solution ($\omega > 0$). From (4-17) we obtain

$$\omega\tau = \cos^{-1} \left(\frac{-1 - \tau_p \ \alpha}{B \ e^{-\alpha\tau}} \right). \tag{4-20}$$

According to this equation, fluctuations originate ($\alpha = 0$) at $B = 1$, in which case they have a period $2\pi/\omega = 2\tau$. This result applies to a hypothetical heat pipe with zero mass since we must have $\tau_p = 0$ to satisfy Eq. (4-18) and hence allow such a solution. In the opposite limit of a massive heat-pipe ($\tau_p \gg 1$), oscillations originate ($\alpha = 0$) only if $B \gg 1$, in which case we see from Eq. (4-20) they have a period $2\pi/\omega = 4\tau$, and from Eq. (4-18) the necessary value of B is $\omega\tau_p$.

37

Since B is proportional to the gas-blocked volume, the fact
that B has a critical value at the onset of unstable oscillations suggests
that a critical gas-blocked volume V_{cr} exists. For a zero-mass heat pipe
($\tau_p = 0$), which has a critical value B = 1, we have from Eqs. (4-11 and 4-12)

$$V_{cr} = z_0 \, A_c \, \frac{\mathscr{R} T_s}{h_{fg} M} \, \frac{T_s}{T_0 - T_s} \quad \text{(massless heat pipe)}, \qquad (4\text{-}21)$$

whereas for a massive heat pipe ($\tau_p \gg 1$), which has a critical value
B = $\omega\tau_p$, we have from Eqs. (4-11), (4-7) and (4-18)

$$V_{cr} = \frac{A_c}{UP} \left[m_e c_e + m_a c_a + m_c \; \left(z_0/L_c\right) c_c \right] \left(\frac{\pi}{2\tau}\right)\left(\frac{\mathscr{R} T_s}{h_{fg} M}\right) \frac{T_s}{T_0 - T_s}. \qquad (4\text{-}22)$$

$$\text{(massive heat pipe)}$$

Fluctuations in a heat pipe with gas-blocked volume smaller than its
critical volume are damped, whereas the converse is true if the gas-
blocked volume is larger. From the above expressions we see that a
heat pipe becomes increasingly more unstable as the active condenser
length z_0 approaches zero. In fact, our simplified theory predicts that
the massless heat pipe will be unstable even with a small gas reservoir since
as $z_0 \to 0$, $V_{cr} \to 0$. A low sink temperature is also a destablizing factor, that
is, V_{cr} is more likely to fall below the gas-blocked volume if $T_s \ll T_0$.
For a massive heat pipe, the critical volume is inversely proportional
to the time lag. Therefore, a short time lag favors stability. The
time lag can be decreased by increasing the gas diffusivity if either
Item 1 or 2 of Table 4-1 governs or by decreasing the wall thickness or
conductivity if Item 2 governs.

When τ_d is non-zero in Eq. (4-13) much the same reasoning
applies, but V_{cr} is increased. Approximately, the critical volume is
given by

$$V_{cr} = z_0 \, A_c \, \frac{\pi \left(\tau_p + \tau_d\right)}{2\,\tau} \left(\frac{\mathscr{R} T_s}{h_{fg} M}\right) \frac{T_s}{T_0 - T_s}. \qquad (4\text{-}23)$$

Since both τ_p and τ_d are inversely proportional to z_0 [Eqs. (4-6), (4-8) and (4-9)], V_{cr} remains finite as z_0 approaches zero. The effect of including the τ_d term in the linearized analysis does not change the preceeding qualitative discussions; it merely increases the size of the critical volume.

The theoretical model may be summarized as follows:

o A diffusion time-lag phenomenon is thought to govern. The re-establishment by diffusion of a convectively distorted vapor-gas front is thought to be the mechanism of the lag.

o The period of instability ranges from 2 to 4 times the diffusion time lag.

o A gas-blocked volume greater than a critical volume V_{cr} is necessary for fluctuations to occur. V_{cr} increases with increasing thermal mass and decreases with decreasing sink temperature.

o The heat pipe tends to be more unstable at low power levels when the active condenser length is small. A massless heat pipe is always unstable at low power, but thermal mass can stabilize at all powers.

o A high mass-diffusivity control gas such as helium and low axially conducting condenser wall such as stainless steel favor stability.

4.2   Experimental Measurements of Pressure Fluctuations

The theoretical model of pressure fluctuations is based on a
diffusive time lag in the establishment of a vapor-gas front in response
to a change in vapor temperature. As a crucial qualitative test of the
model, a series of pressure-fluctuation measurements were made with
a heat pipe containing as the control gas first argon, which has a
relatively low diffusivity and then helium, which has a relatively high
diffusivity. The diffusive time lag for helium should be much shorter
than the lag for argon; thus if the postulated model is correct, the
change of control gas should have a marked effect on the fluctuations.

The specifications of the test setup are contained in Table 4-2.
The heat pipe used for the experiment was a stainless-steel two-artery
slab-wick design, 62.75 inches long and 0.5 inches in diameter. The arteries
were never primed during the tests, but sufficient heat-transfer capacity
in excess of 80 watts was obtained in a level orientation.

Pressure fluctuations were measured with a 5-psia
differential pressure transducer, both sides of which were connected to
the feed tube in the heat-pipe reservoir. One leg of the connection is
fitted with a valve that is closed when measurements are being made and
open otherwise. The output from the transducer is recorded with a strip-
chart recorder. Runs were made at low power, in which case the gas front
extends into the adiabatic section, and at intermediate power, in which
case the front is in the condenser.

Typical fluctuation measurements are shown in Figs. 4-1 and
4-2. With argon at the low-power of 3 watts (Fig. 4-1), the pressure
trace varied slowly and randomly, typically at a rate of $\pm$ .05 psi/minute
except at discrete points when the trace suddenly recorded a marked rise
or fall of approximately .35 psi in less than half a minute. Such an
isolated surge is shown in the Figure (4-1). Only two surges were
recorded in a 31 minute interval. At a higher power of 10 watts, the
front was still in the adiabatic section, and while the trace is similar
to that at 3 watts, six isolated surges were recorded in 44 minutes. These
surges alternately increased and decreased. In comparison, at the low

40

Table 4-2.

Specifications of the Test Setup

for Pressure Fluctuation Measurements

Heat-pipe dimensions (all materials stainless steel):

Outside diameter	-	0.5 inches
Wall thickness	-	0.028 inches
Internal grooves	-	150/inch
Evaporator length	-	23 inches
Adiabatic length	-	16.75 inches
Condenser length	-	25 inches
Cross-sectional area of vapor space	-	.1064 square inches
Reservoir volume	-	8.72 cubic inches
Arteries (2)	-	.063 inch I.D.
Wick		.050 inch slab

Test conditions:

Thermal resistance between condenser saddle and heat sink -	1/32 x 1.5 x 25 inch Teflon.
Condenser saddle -	.1275 lb_m/inch of aluminum.
Set point -	with the sink and reservoir at 10°F, sufficient gas was added to give a 70°F vapor temperature at 67 watts.
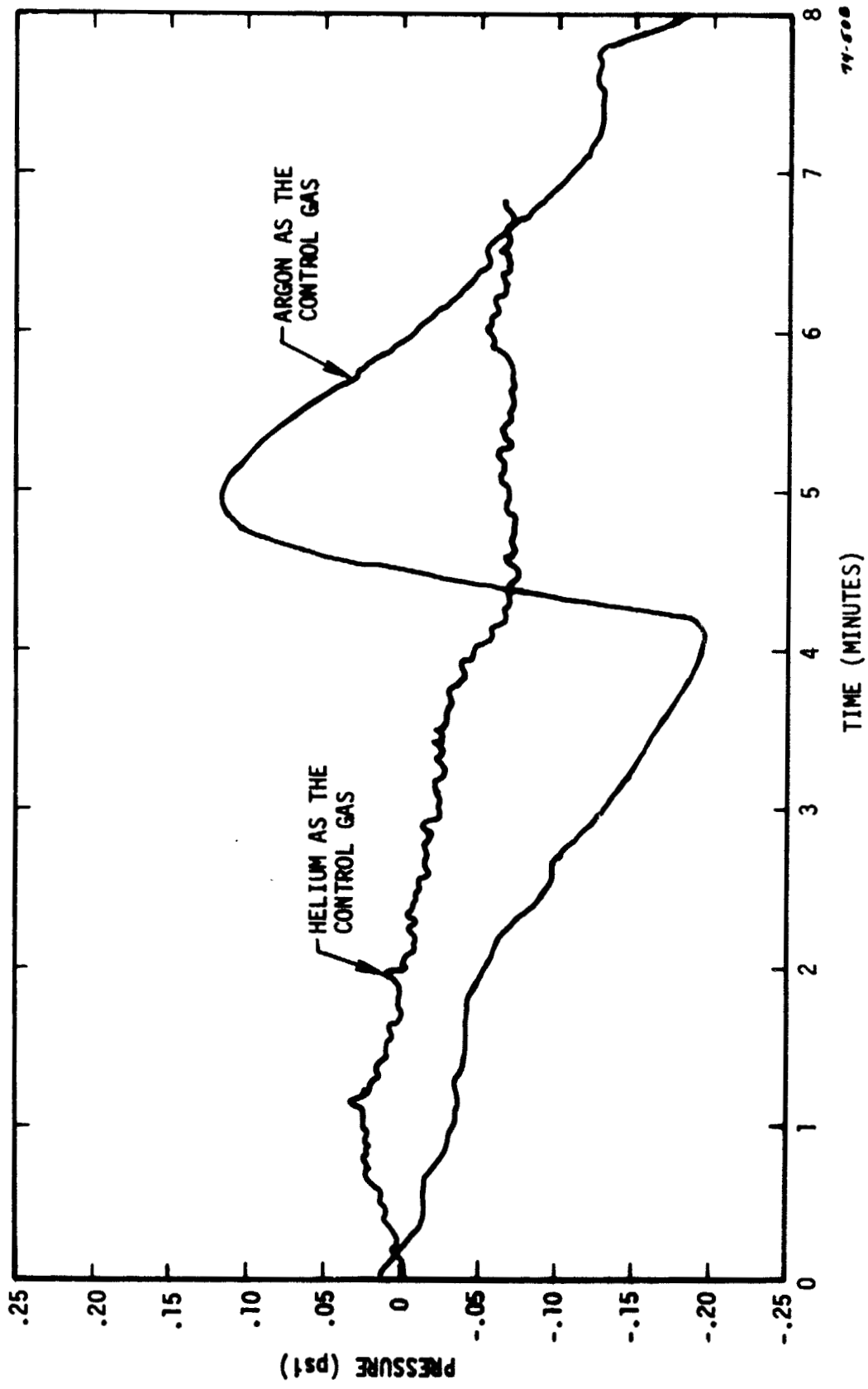
FIGURE 4-1. Pressure fluctuations at low power (3 watts) with the vapor-gas front in the adiabatic region.
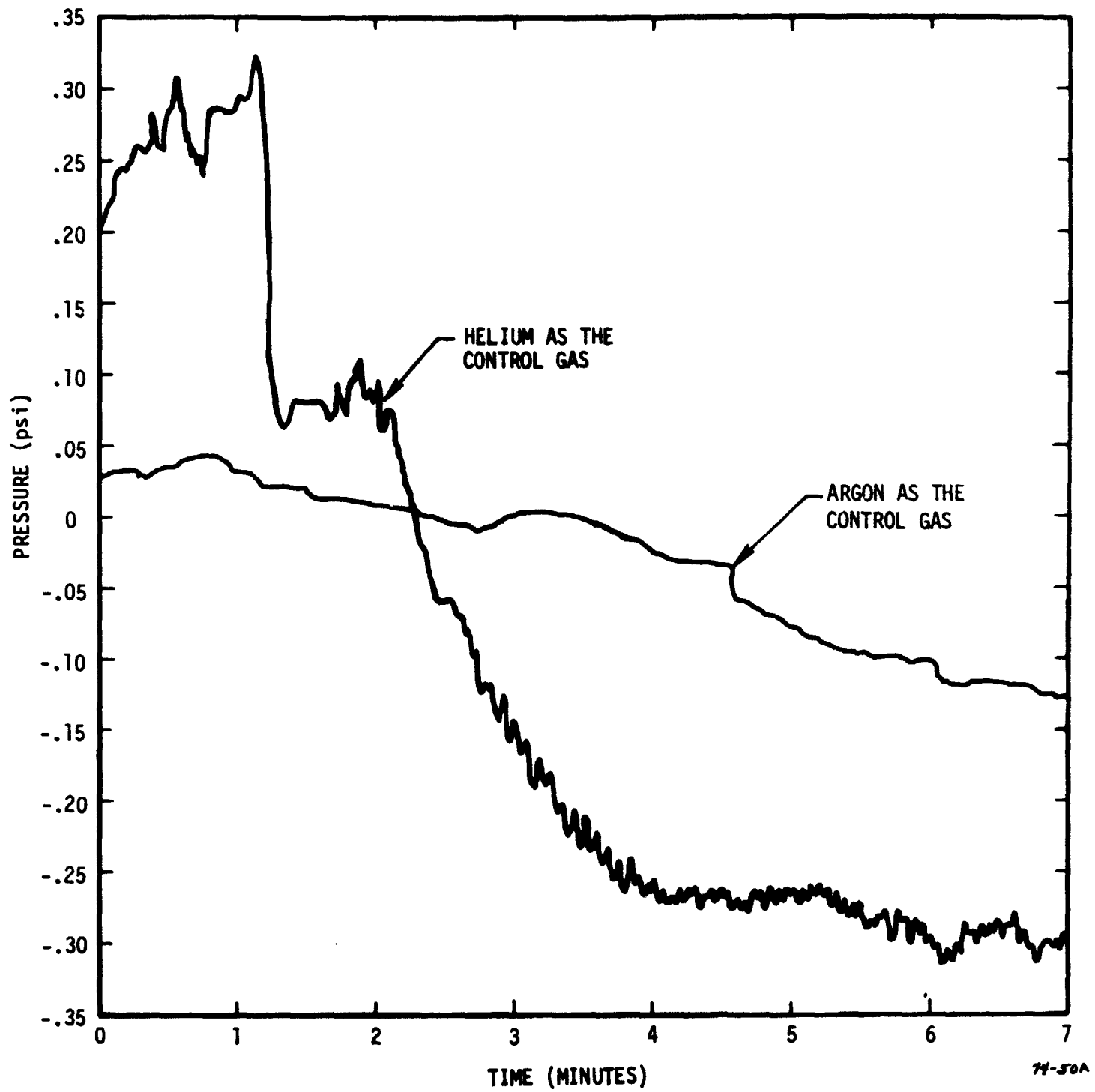
FIGURE 4-2. Pressure fluctuations at higher power (67 watts) with the vapor-gas front in the condenser region.

power of 3 watts with helium as the control gas, no surges were observed.
However, as seen in Fig. 4-1, the trace is characterized by fairly regular
oscillations of about 7 cycles per minute around a randomly varying mean
pressure.

At the higher power, 67 watts, in which case approximately one
fourth of the condenser is active, the situation is somewhat reversed.
As seen in Fig. 4-2, no surges were observed with argon, however, some
were observed with helium. Also, the oscillations with helium are more
pronounced and of a higher frequency (17 cycles/minute) at the higher
power.

The primary conclusion of the experimental measurements is
that the type of control gas, as the theory predicts, has a marked effect
on the fluctuations. This strongly suggests that a diffusion time lag plays
a crucial role in the fluctuation mechanism. We cannot conclude, however,
that pressure fluctuations are well understood. For example, we observed
pressure surges, that have no counterpart in the theoretical model. Further
experimental research is required to verify the key physical parameters that
effect the fluctuations and to assess the magnitude of fluctuations that
can be tolerated without interfering with arterial operation. It may then
be possible to design an arterial variable-conductance heat pipe with
ammonia as the working fluid.

4.3   Priming Studies with a Glass Heat Pipe

A method has been developed at TRW to prevent entrapment of
a gas bubble during arterial priming. The noncondensable gas is vented
through capillary-size holes in a foil-walled section of artery at the
evaporator end. Liquid cannot plug the holes in the foil and thus prevent
venting, because the foil is sized so thin that the menisci on either side
of a potential plug would coalesce.

Part of our research task was to fabricate a glass heat pipe
and use it to study priming with this new approach. Several aspects of
arterial priming can effectively be studied with a glass heat pipe. For
example, venting gas at the evaporator end of the artery relies on priming
proceeding uniformly from the condenser end to the evaporator end. If
a bubble is trapped at some position along the artery other than at the

evaporator end, then it would first have to be convected to that end before it could vent. Convection of a bubble for various heat loads can be observed directly with the glass heat pipe. Another process to be studied is priming under a load. For a given evaporator elevation, we can use the glass heat pipe to find the maximum heat load under which priming will occur. Other details of the priming process can be studied such as the minimum capillary hole size in the foil that will still vent gas, and whether in some circumstances, the foil-walled portion of the artery can be flooded by a pool of excess liquid and hence be unable to vent gas. We were unable to answer these crucial questions because funds on the contract were exhausted before the studies could be carried out.

Fabrication of the apparatus is essentially complete. As shown in Fig. 4-3, the main structure consists of a 0.752 in. O.D. and 0.515 in. I.D. glass tube, 43 inches long, with machined stainless-steel end fittings. The heat pipe is held in a plexiglass cradle, which also serves as a safety shield when ammonia is used as the working fluid.

The heat pipe is designed for study of the arterial/slab-wick configuration. Cross sections in the evaporator and condenser sections are shown in Fig. 4-4. The artery is mounted on one side of the slab wick, and a 1/8-inch diameter stainless-steel sheathed heater with a 12-inch heated section is inserted into a double-layer screen casing that is spot welded to the other side of the wick. The unheated end of the heater passes through and is brazed into the evaporator end cap. In the condenser region, a stainless-steel cooling loop extends along the opposite side of the wick as the artery. It passes through and is brazed into the condenser end cap. A 1/16-inch O.D. stainless-steel sheathed thermocouple extends into the adiabatic section so the vapor temperature can be monitored. A feature of this design is that it closely models actual arterial/slab-wick heat pipes such as the ones to be used in the rocket-flight experiment as described in the next section.
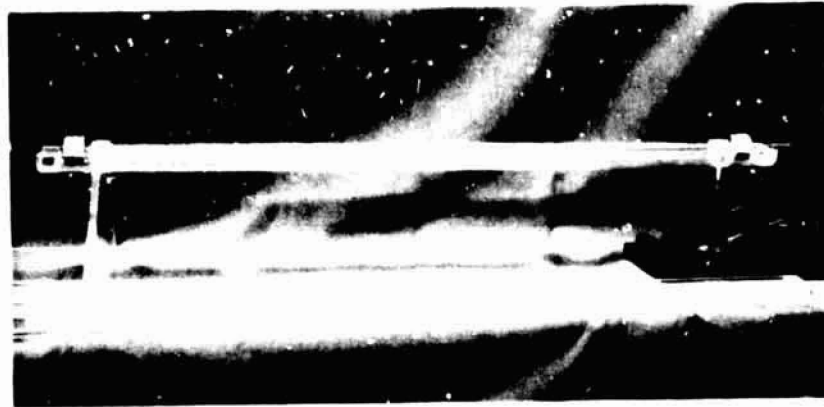
FIGURE 4-3. Glass heat-pipe apparatus
with safety shield removed.
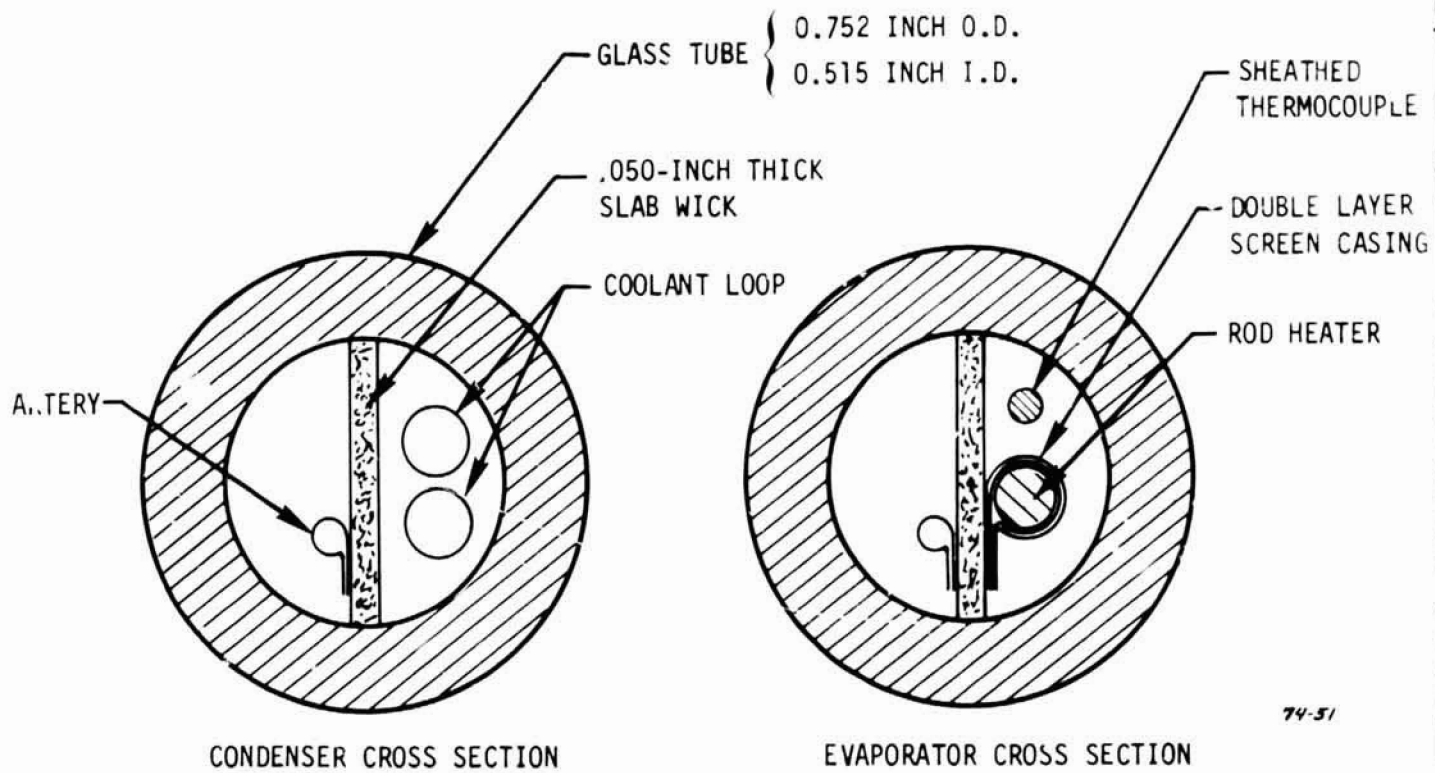
FIGURE 4-4. Cross section of the glass heat pipe in
the condenser and evaporator regions.

5.0   SOUNDING-ROCKET EXPERIMENT

The GSFC sounding-rocket heat-pipe experiment scheduled for
1974 provides a unique first opportunity for a zero-gravity test of
the mechanism of menisci coalescence to vent noncondensable gas during
arterial priming. Part of our research task was to design, fabricate
and test two research heat pipes (and two spares) for the flight
experiment.

The experiment is especially challenging in that only six
minutes in zero gravity are available for priming and then applying
a heat load to verify that a primed state was achieved. In addition,
there are uncertainties as to whether the so-called "pogo effect" will
interfere with priming. If, at the instant of rocket-engine shut-down,
a surge of excess liquid arrives at the evaporator before the artery
primes, the evaporator end of the artery may fill with liquid and prevent
venting. Our task is not only to test whether or not the heat pipe primes,
but also to obtain some crucial information on the internal conditions of
the heat pipe during the experiment. Thus, each heat pipe has one of two
otherwise identical arteries instrumented at the evaporator end with a
miniature thermistor. The thermistor, which is electrically heated, is
markedly cooler when submerged in liquid than when in vapor. As such, it
detects the presence or absence of liquid in the priming foil. In this
way, the research heat pipes are designed to overcome a nagging difficulty
of arterial heat pipes, that of diagnosing the cause of unsuccessful priming.
Priming failure can have several causes, however, they generally fall into
one of two categories listed below.

Two Categories of Priming Failure

1. Evaporator stress too high for priming due to

        o   insufficient fluid in the heat pipe
        o   too large a residual heat load during priming

        o   too large of a hydrostatic load due to adverse
            orientation in an acceleration field

47

2. Entrapment of noncondensable gas due to

    o   failure to vent the gas through the priming foil

    o   a gas bubble at some location in the artery
        other than the evaporator end.

If, during the priming period, liquid is not detected at the evaporator end of the artery, then priming failure is attributed to the first category, excessive evaporator stress.[1] If, on the other hand, liquid is detected, we conclude that the stress was low enough for priming to take place, and a subsequent failure of the uninstrumented functional artery is attributed to the second category, entrapment of noncondensable gas.

The thermistor instrumentation also provides a means of verifying that a sufficient heat load is applied when we test for the primed state of the functional artery. If the thermistor detects that liquid recedes (which it should, due to the large pore in the instrumented artery), then the heat load is sufficient to empty the functional artery if priming is unsuccessful. If subsequently a burnout does not occur, then the primed state of the functional artery is verified.

The diagnostic logic is summarized in Figure 5-1. The heavy line represents successful priming and verification of such.

5.1   Description of the Heat Pipes

As shown in Figure 5-2, the heat pipes are of an arterial/slab-wick configuration. Their specifications are listed in Table 5-1. The two heat pipes to be used in the flight experiment differ only in the details of their priming foils. For the heat pipe designated X-2, the active length of the priming foil is 1.5 inches, the holes are in spiral rows, and the end on the functional artery is crimped closed, whereas for the heat pipe designated X-1, the active length is 0.375 inches,

---

1. A relative large pore of comparable size to the artery diameter is provided just behind the thermistor to insure that gas vents from the instrumented artery.
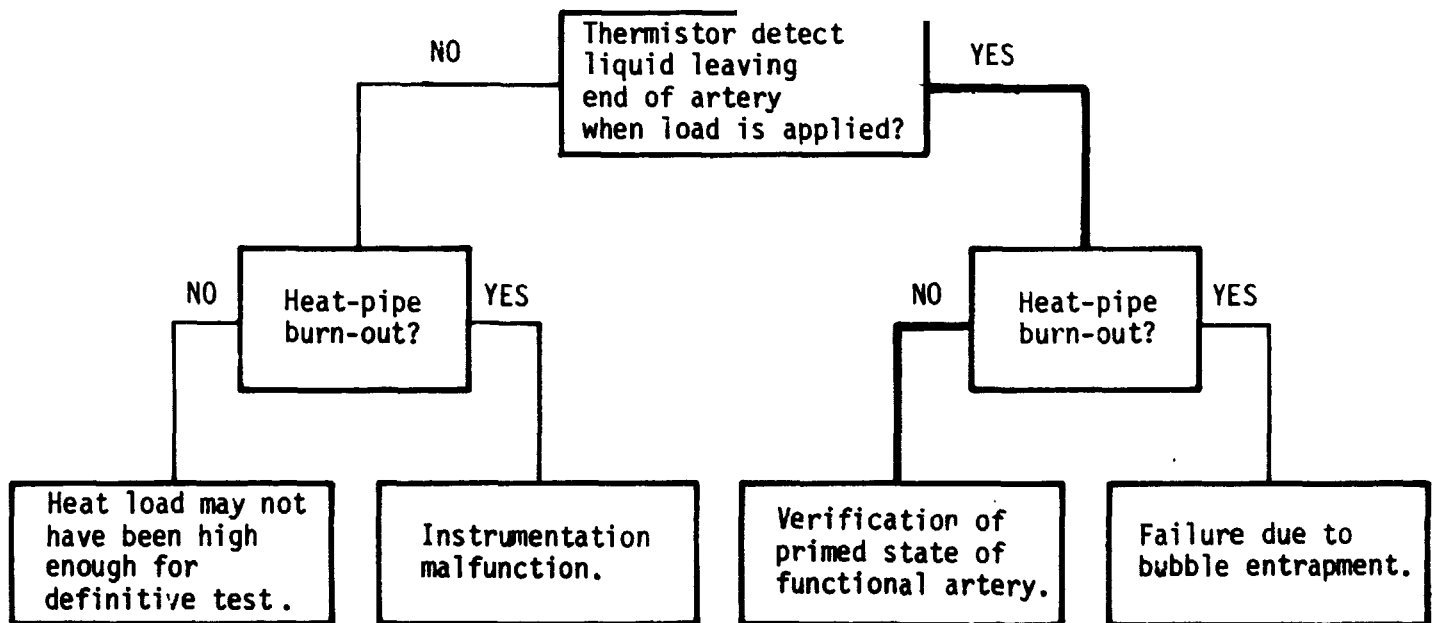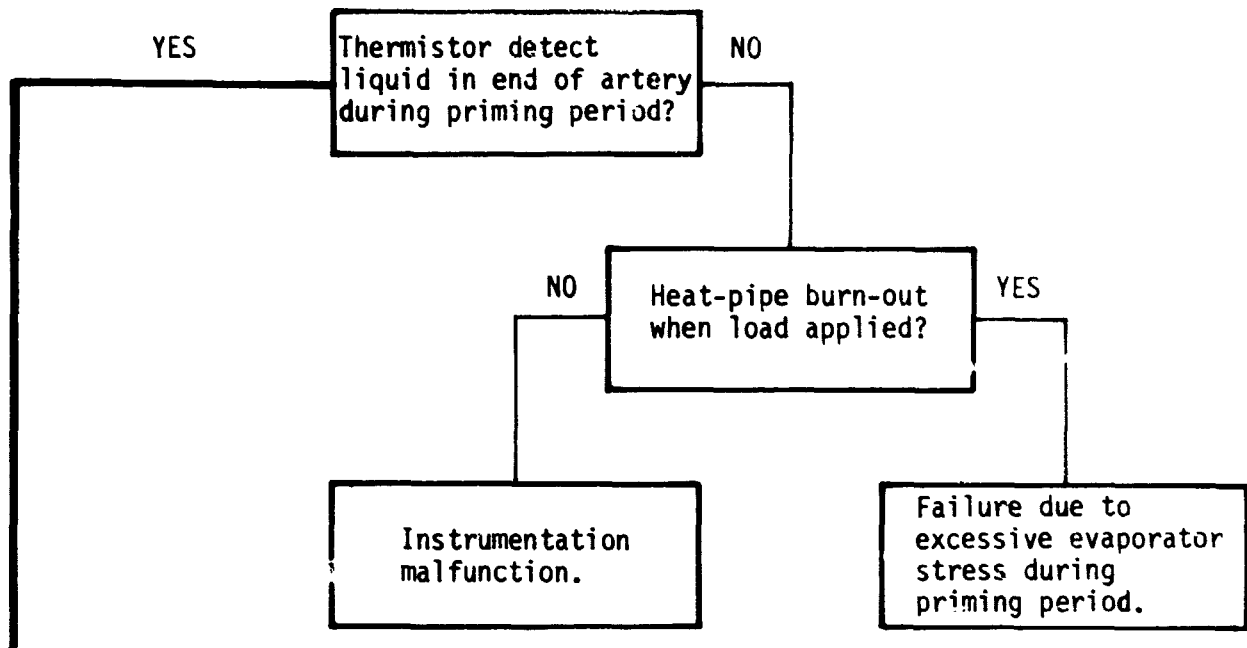
FIGURE 5-1. Summary of diagnostic logic for the flight experiment.

FEED TUBE

SLAB WICK

SCREEN
ARTERY

A

A

.028"

.170"

.050"

.5"O.D.

.063"I.D.

SECTION A - A

THERMISTOR

PRIMING FOIL

ELECTRICAL
FEED-THROUGH

TEFLON THERMISTOR HOLDER
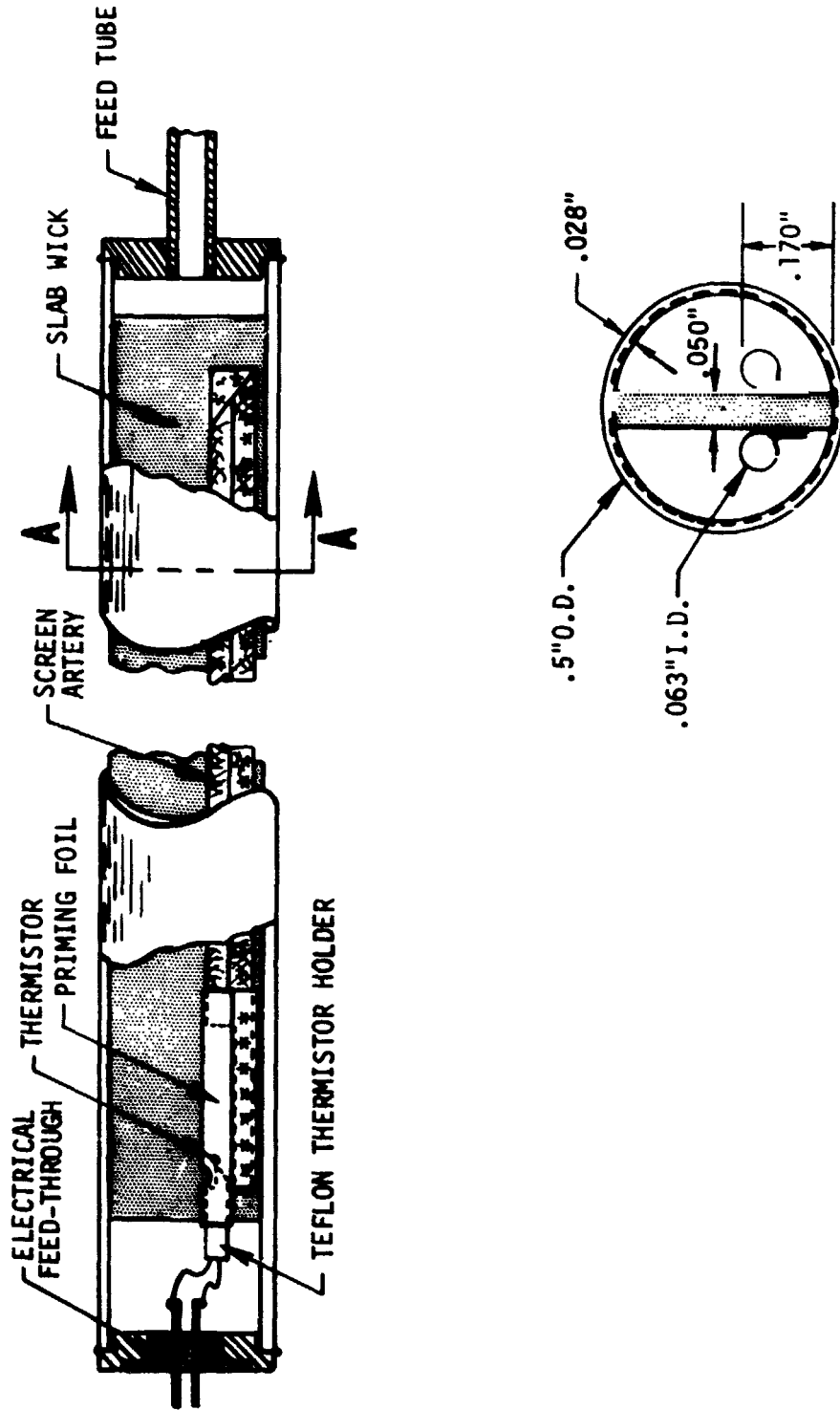
FIGURE 5-2. Configuration of the flight heat pipe.

TABLE 5-1

SPECIFICATION OF THE RESEARCH HEAT PIPES

Tube (304 stainless-steel):
    Length - 36 inches
    Outside diameter - 0.5 inches
    Wall thickness - 0.028 inches
    Internal threads - 150 per inch

Slab-wick (304 stainless-steel X-13 felt metal):
    Thickness - 0.050 inches
    Fiber diameter - 0.00085 inches
    Porosity - 84%

Arteries (304 stainless-steel 150-mesh screen):
    Inside diameter - 0.063 inches
    Height from bottom of slab wick - 0.170 inches

Priming foils (304 stainless-steel):
    Thickness - 0.0005 inches
    Diameter of holes - 0.010 inches
    Hole spacing in row - 0.032 inches
    Row spacing - 0.075 inches
    Active length $\begin{cases} 1.50 \text{ inches for Configuration X-2} \\ 0.375 \text{ inches for Configuration X-1} \end{cases}$
    Hole pattern $\begin{cases} 17° \text{ spirals for Configuration X-2} \\ \text{straight for Configuration X-1} \end{cases}$

TABLE 5.1 (cont.)

Thermistor (Veco, part No. 32A7):
Bead diameter - .013 inches
Leads - .001 inch platinum
Resistance at 25°C - 2000 Ω

Flight heat sink: aluminum block 12" X 1.32" X 1.32"
Flight heater: 10 inches long and beginning 2 inches
from the evaporator end

Flight thermistor locations:

Thermistor No.	Distance from evaporator end
1	3 inches
2	7
3	16
4	20
5	25
6	30
7	35
8	on heat sink
9	on heat sink

the holes are in straight rows and the end is closed with a plug. The X-2 configuration priming foil is a design similar to that used on the Canadian Technology Satellite (CTS) program. The X-1 configuration priming foil is an experimental design that represents an attempt to improve the ruggedness and minimize the chance of trapping a gas bubble in the last instant of priming the foil itself.

The instrumentation consists of a bead-type thermistor that is held at the apex of the conical end of a cylindrical teflon plug, (.073-inch diameter, .4-inch long) which in turn fits into the end of one of the priming foils. The .001-inch platinum leads from the bead pass through two 0.008" diameter holes that run the length of the plug. The plug is held in the end of the priming foil by a band of heat-shrink tubing. The thermistor leads are connected to the prongs of an electrical feed through in the heat-pipe end cap with 0.007-inch nickel wire. Connections are made with spot welds. The nickel wire is mechanically secured to the outer end of the teflon plug with another band of heat-shrink tubing.

5.2 Fabrication Highlights

Some problems arose during fabrication, which are discussed here so they can be avoided in future projects.

We originally planned to use a miniature hot-wire probe instead of a thermistor as the liquid sensor. During the breadboard test, however, we discovered that methanol attacked the solder that secures the hot-wire element to the support prongs. After a 12-hour submersion in methanol, the hot wire detached. At this point we decided to use a thermistor.

Because of the incompatibility of methanol and solder, we could not solder the electrical feed-through into the heat-pipe end cap. We tried heli-arc welding, but the heat generated resulted in the cracking of the glass insulation. Laser welding, which generates little heat, was also tried, however, we found that the weld bead had microscopic cracks that resulted from the dissimilarity of inconel of the feed-through and the stainless-steel end cap. The solution was the use of a pure-lead braze after both parts were first gold plated. As a final assembly step, the end cap was laser welded to the heat pipe.

Another problem occurred as the result of vacuum firing. Since we did not want to subject the thermistor installation to the vacuum-firing temperature, we planned to vacuum fire before the thermistor was installed. The evaporator end of the wick was left extended approximately one inch from the tube, the heat pipes were vacuum fired, and the thermistor was installed. We then planned to pull the wick the final distance into the tube in the usual manner, however, vacuum firing resulted in seizure. Only after pulling with excessive force, were we able to pull a wick into one of the heat pipes. The other three heat pipes were completed by cutting off the condenser end of tube and welding a short piece of tube to the evaporator end with the use of a sleeve over the joint.

5.3   Fill Determination

An initial fluid fill of .0390 lb_m of methanol was calculated by TRW's MULTIWICK computer program to give the maximum heat load under which priming will occur in zero gravity without a vapor-space slug. MULTIWICK also calculated that .0390 lb_m of methanol would be more than sufficient to prime in earth gravity. In the computer calculations, however, we did not take into account an effect that was observed in a sub-scale glass-tube priming test; that the stress required to prime the foil-walled portion of an artery is somewhat lower than that required to prime the screen-walled portion. In initial tests, priming was difficult to achieve. The problem was solved by increasing the amount of methanol to .0487 lb_m. This amount corresponds to the maximum in zero gravity that will not result in a vapor-space slug with zero heat load. Under load, however, some slugging will occur.

Since the experiment concerns priming in the presence of non-condensable gas, 1.87×10^{-9} lb moles of a mixture of 90% nitrogen and 10% helium were added to each heat pipe. This amount results : approximately one-inch of condenser blockage.

5.4   Steady-State Capacity Tests

Steady-state capacity tests were carried out and the results are summarized in Figure 5-3. The theoretical predictions based on MULTIWICK are shown as well. Each of the four heat pipes were tested with primed arteries at 1.0-inch and 0.25-inch elevations, however,
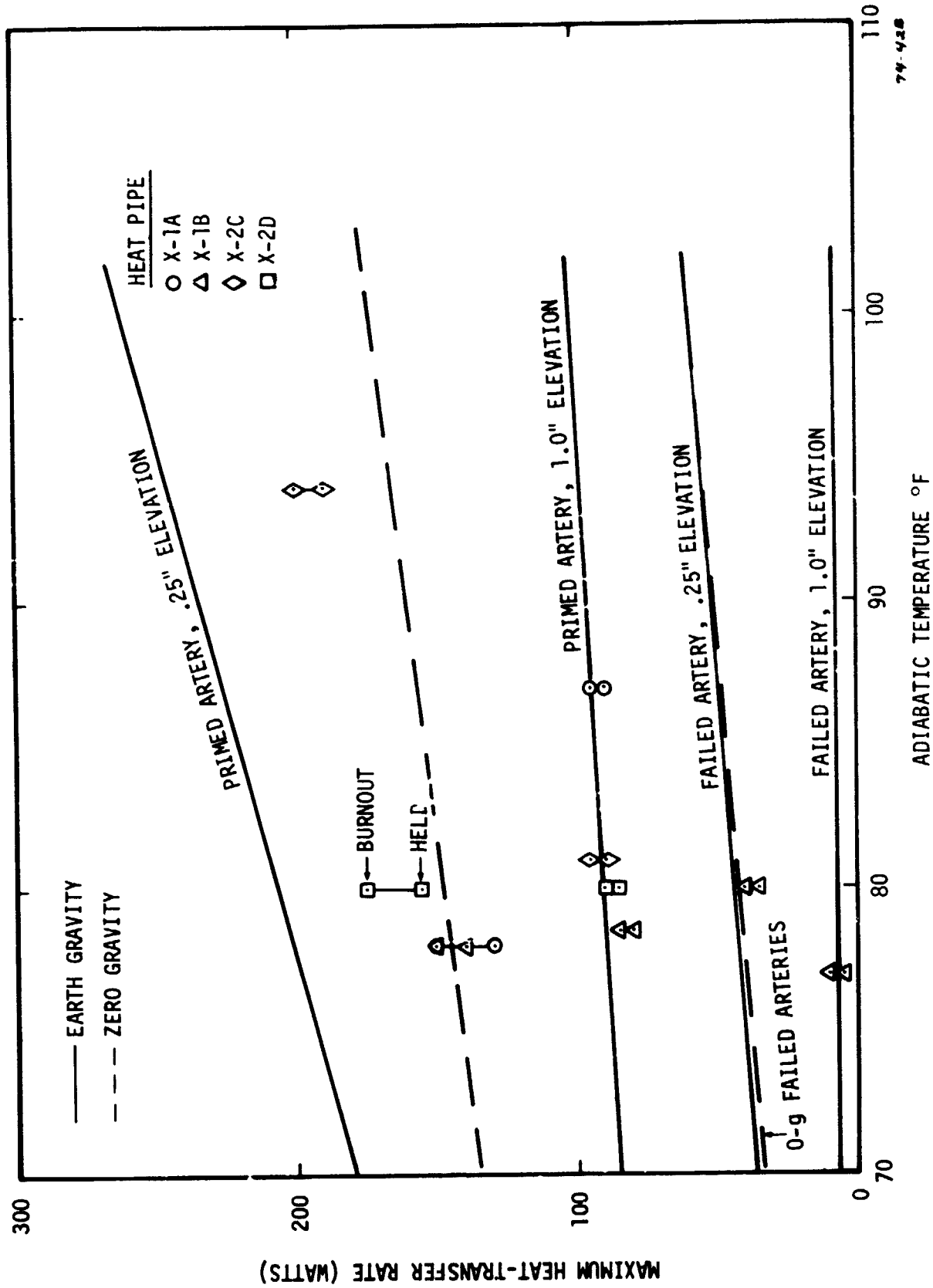
FIGURE 5-3. Results of steady-state tests and theoretical predictions.

only one was tested with failed arteries. Agreement between the theoretical predictions and the experimental results are generally good except in the case of 0.25-inch elevation where predictions are generally too high by 20%.

5.5 Priming Tests with the Thermistor Instrumentation

The electronic circuit for the thermistor is particularly simple; it consists of a 3000-ohm resistor and a 28-volt power supply in series with the thermistor. The circuit output is the voltage across the thermistor. The output voltage is approximately 3.7 volts when the arteries are primed and 1.2 volts when deprimed. Sometimes, however, in the primed state boiling occurs at the bead, in which case the output oscillates rapidly about some mean voltage greater than 3.5 volts. In the deprimed state, discrete intermediate output voltages occur that are attributed to partial cooling of the thermistor bead by small liquid fillets around it. With sufficient evaporator stress these fillets are not replenished from neighboring liquid and they evaporate, which results in the low 1.2-volt output. Typically, when the artery deprimes by, say, elevating the evaporator end, the output voltage first drops from 3.7 volts to an intermediate valve of 2.4 volts, and then again to 1.2 volts after the fillets evaporate.

Priming tests were carried out by slowly lowering the evaporator end of the heat pipe in 0.1-inch steps until the output voltage from the heat pipe indicated that a primed state was achieved. To check that the uninstrumented functional artery had also primed, 75 watts were applied, which results in a burnout if it had not. Of the four heat pipes, in two (X-1A and X-2C) the functional arteries had not yet primed. Further testing showed that a lower evaporator elevation by approximately 0.2 inches was required to prime the functional arteries in these cases. These discrepencies can be attributed to the differences incurred during fabrication of the arteries, and the effect mentioned earlier (Section 5.3) of the reluctance of the liquid in the screen-walled portion of the artery to enter the foil-walled portion. In the case of heat pipe X-2C, the effect of thermistor cooling by liquid fillets around the thermistor appears to be greater than the other heat pipes to the extent that it is not clear whether the thermistor is detecting a primed state or fillets. Based on the above considerations, we have recommended that heat pipes

X-1B and X-2D be designated as the primary ones for flight. The back-up heat pipes X-1A and X-2C have been recommended for the qualification vibration tests.

5.6   Transient Tests with the Flight Power Profile

The power profile to be used in the experiment is shown in Figure 5-4 below:
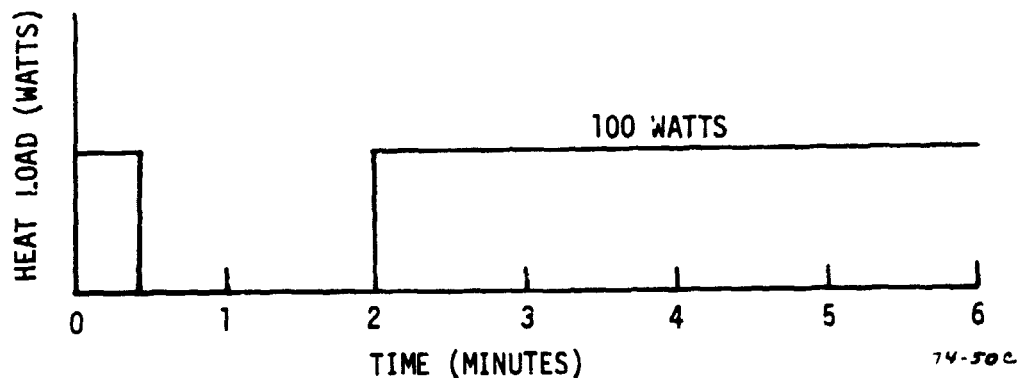
FIGURE 5-4. Power profile for the flight experiment.

The duration of the zero-gravity period is expected to be 6 minutes. During the first half minute, 100 watts is applied to move excess liquid to the condenser end of the heat pipe. This amount of heat is sufficient to transfer 12% of the total amount of methanol. The zero-power period from t=.5 minutes to t=2 minutes is for priming. During the remainder of the zero-gravity period, 100 watts are again applied. If the functional artery has not sucessfully primed, a burnout will occur.

Each heat pipe was tested repeatedly in the laboratory with the proposed power profile. To eliminate the contribution of puddle flow, which is not present in zero-gravity, the evaporator end of the heat pipe is elevated .5 inches for the final 100-watt period. During the transient tests, both temperature and thermistor voltage were recorded. The result of the transient test for heat pipe X-2D is shown in Figure 5-5.

Initially the evaporator end is raised approximately 10 inches to ensure the arteries are in an unprimed state. At t=0 minutes, the heat pipe is leveled and 100 watts is applied. The vapor temperature responds rapidly to the heat input and the thermistor voltage remains low,

57
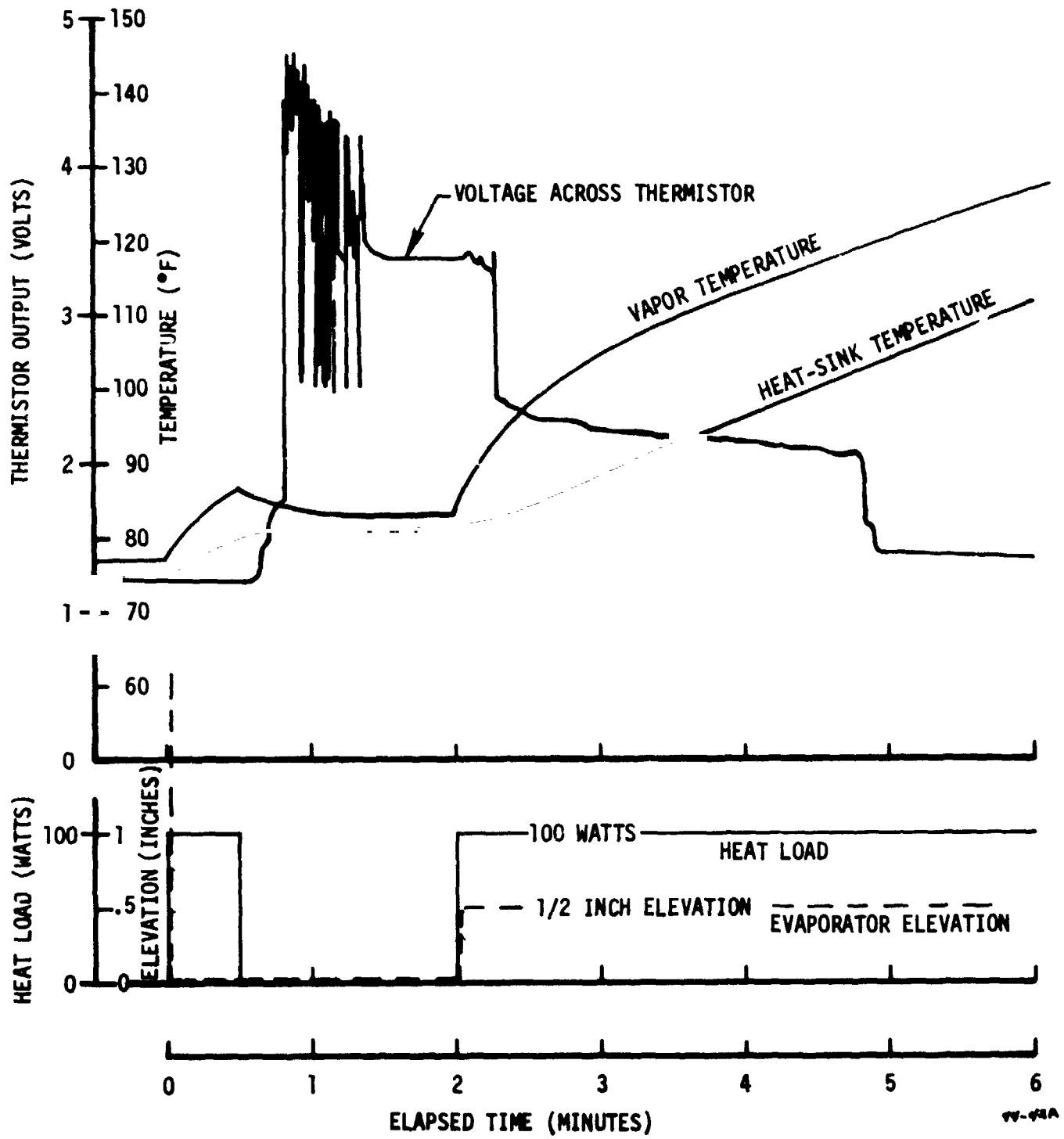
FIGURE 5-5. Results of the transient test of heat pipe X-2D.

indicating that the arteries are remaining unprimed. At t=.5 minutes
the heat load is dropped to zero. The thermistor output voltage begins
to climb as fillets form around the thermistor bead. Then abruptly at
t=.8 minutes, the instrumented artery primes. Film boiling occurs at
the thermistor bead, as evidenced by the oscillations until t=1.3 minutes.
At t=2 minutes, 100 watts is applied and the evaporator is elevated to
.5 inches. At t=2.3 minutes the instrumented artery deprimes, as evidenc-
ed by the step drop in thermistor voltage. The functional artery continues
to operate, and the temperature difference between the vapor and condenser
attains a steady-state value by t=4 minutes. At t= 4.8 minutes, fillets
around the thermistor bead break away, and the thermistor voltage steps
down again. The test terminates at t=6 minutes.

Several tests were run when the functional artery was
intentionally deprimed after t 2 minutes, and subsequently the evaporator
temperature exceeds 200°F in less than one minute.

5.7 Real-Time Power Profile Override

We will have the opportunity to monitor data from the heat pipes
during the flight and, if necessary, override the preprogrammed power
profile. The data to be monitored is:

o   Evaporator temperature T_1 measured by
    thermistor No. 1 (located 3 inches from
    the evaporator end).

o   Adiabatic temperature T_3 measured by thermistor
    No. 3 (located 16 inches from the evaporator
    end).

o   The voltage V_{TH} across the thermistor.

The real-time control we require is to override the programmed power
profile with a zero-power command for any desired time interval. The
override will be exercised if certain conditions appear as the data is
monitored. A list of the most probable anomalies is given below:

1. $V_{TH} \cong 0$ (thermistor shorted).

2. $V_{TH} \cong 28$ volts (thermistor lead broken).

3. It takes longer than 2 minutes for V_{TH} to jump and indicate a primed state.

4. A prime is indicated ($V_{TH} > 3$ volts) at $t = 0$.

5. An artery dump (drop in V_{TH}) is not indicated.

6. V_{TH} is at some intermediate value or fluctuates in such a way that it is difficult to interpret.

7. $T_1 - T_3$ is not equal to zero at $t = 0$.

8. $T_1 - T_3$ does not drop to zero by $t = 2$ minutes.

9. A burnout occurs after $t = 2$ minutes, ($T_1-T_3 > 20°F$)

10. $T_1 - T_3$ may continuously increase after $t = 2$ minutes but not exceed 20°F.

Of the above anomalies, we want to override the programmed power profile in three cases: Nos. 3, 8 and 9 above. The response to these anomalies are as follows:

Anomaly	Response
3	If V_{TH} does not rise above 3.0 volts by $t = 2$ minutes, extend zero-power period to $t = 3$ minutes or until V_{TH} does exceed 3.0 volts.
8	If ΔT is greater than 3°F at $t = 2$ minutes, extend zero-power period to $t = 3$ minutes or until ΔT is less than 3°F.
9	If, after $t = 2$ minutes and before $t = 4$ minutes, ΔT exceeds 20°F, then command zero power until $t = 5$ minutes.

The first two responses above extend the priming period an extra minute if there is evidence that conditions for priming have not been achieved. The last response is an attempt at a second try to prime the arteries if a burnout occurs.

6.0   REFERENCES

Section 1.0:

1-1   B. D. Marcus, "Theory and Design of Vraiable Conductance
       Heat Pipes: Hydrodynamics and Heat Transfer", Research
       Report No. 1, TRW Report No. 13111-6021-R0-00, April 1971.

1-2   B. D. Marcus, "Theory and Design of Variable Conductance
       Heat Pipes: Control Techniques", Research Report No. 2,
       TRW Report No. 13111-6027-R0-00, July 1971.

1-3   B. D. Marcus, "Theory and Design of Variable Conductance
       Heat Pipes", NASA CR-2018, April 1972.

1-4   B. D. Marcus and G. L. Fleischman, "Steady-State and
       Transient Performance of Hot Reservoir Gas-Controlled
       Heat Pipes", ASME Paper No. 70-HT/SpT-11, 1970.

1-5   D. K. Edwards and B. D. Marcus, "Heat and Mass Transfer
       in the Vicinity of the Vapor-Gas Front in a Gas Loaded
       Heat Pipe", ASME Jour. of Heat Transfer, Vol. 94,
       Ser. C, No. 2, pp 155-162, 1972.

1-6   D. K. Edwards, G. L. Fleischman and B. D. Marcus, "Theory
       and design of Variable Conductance Heat Pipes: Steady
       State and Transient Performance", Research Report No. 3,
       NASA CR-114530, December 1972.

1-7   B. D. Marcus, D. K. Edwards, W. T. Anderson, "Variable
       Conductance Heat Pipe Technology", Research Report No. 4,
       TRW Report No. 13111-6055-RU-00, December 1973.

1-8   B. D. Marcus, D. K. Edwards and G. L. Fleischman,
       "Diffusion Freezeout in Gas-Loaded Heat Pipes",
       ASME Paper No. 72-WA/HT-33, 1972.

1-9   J. P. Kirkpatrick and B. D. Marcus, "A Variable
       Conductance Heat Pipe Flight Experiment", Fundamentals
       of Spacecraft Thermal Design, Prog. Astronautics and
       Aeronautics, Vol. 29, John W. Lucas, Ed., p. 505, 1972.

1-10   J. P. Kirkpatrick and B. D. Marcus, "A Variable Conductance
       Heat Pipe/Radiator for the Lunar Surface Magnetometer",
       Thermal Control and Radiation, Prog. Astronautics and
       Aeronautics, Vol. 31, Chang-Lin Tien, Ed., p. 83, 1973.

1-11   B. D. Marcus, "Ames Heat Pipe Experiment (AHPE) Experiment
       Description Document", NASA CR-114413, January 1972.

1-12   D. K. Edwards, G. L. Fleischman and B. D. Marcus, "User's
       Manual for the TRW Gaspipe Program", NASA CR-114306,
       April 1971, and "User's Manual for the TRW Gaspipe 2 Program",
       NASA CR-114672, October 1973.

Section 2.0:

2-1   B. D. Marcus, D. K. Edwards, W. T. Anderson, "Variable
      Conductance Heat Pipe Technology", Research Report No. 4,
      TRW Report No. 13111-6055-RU-00, December 1973.

2-2   W. T. Anderson, "Hydrogen Evolution in Nickel-Water
      Heat Pipes", AIAA 8th Thermophysics Conference, Palm
      Springs, Calif., July 1973, AIAA Paper No. 73-726.

2-3   S. W Petrick, "Hydrogen Gas Generation in Water/Stainless
      Steel Heat Pipes", ASME Winter Annual Meeting, New York,
      November 1972, ASME Paper 72-WA/HT-37.

2-   K. Barton, "Acceleration of Corrosion Tests on the Basis
      of Kinetic Studies of the Rate Controlling Combination
      of Factors", in First International Congress on Metallic
      Corrosion, London, April 1961 (Butterworths, London, 1962).

2-5   B. D. Marcus, "Theory and D.sign of Variable Conductance Heat
      Pipes", NASA CR-2018, April 1972.

2-6   J. Schwartz, "Performance Map of the Water Heat Pipe and the
      Phenomenon of Noncondensable Gas Generation", ASME - AIChE Heat
      Transfer Conference, Minneapolis, Minnesota, August 3-6, 1969,
      ASME Paper 69-HT-15.

2-7   M. Groll, H. Kreeb, W. D. Munzel, and P. Zimmernam, "Per-
      formance and Life .ests of Low Temperature Heat Pipes",
      Fourth International Congress CHSA, Prague, Czechoslovakia,
      September 11-15, 1972.

2-8   F. L. LeQue and H. R. Copson, eds., Corrosion Resistance
      of Metals and Alloys, (Reinhold, New York, 1963).

2-9   D. H. Dazeley, Organic Chemistry, (Cambridge University
      Press, London, 1969).

2-10 L. F. Fiesen and M. Fieser, Organic Chemistry, 3rd ed.,
      (Reinhold, New York, 1956).

2-11 H. Kreeb, "Zur Wahl von Werkstoff and Wärme-träger bei
      Niedertemperature", Ph.D. Thesis, Stuttgart University,
      1972.

2-12 G. A. Nelson, ed., Corrosion Data Survey, (Shell Develop-
      ment Co., Emeryville, Calif., 1954).

2-13 M. Groll, O. Brost, H. Kreeb, K. P. Schubert, and P.
      Zimmerman, "Heat Transfer Limits, Lifetests, and Dynamic
      Behavior of Heat Pipes", International Symposium on Two-
      Phase Systems, Technion City, Haifa, Israel, Aug. 29-Sept. 2,
      1971.

2-14 G. T. Bakhavlov and A. V. Turkovskaya, Corrosion and Protection of Metals, (Pergamon Press, New York, 1965).

2-15 U. R. Evans, The Corrosion and Oxidation of Metals, (St. Martin's Press, New York, 1960).

2-16 T. P. Hoar, "The Production and Breakdown of the Passivity of Metals", in Proceedings of the Third International Congress on Metallic Corrosion, Moscow, May 1966. (MIR, Moscow, 1969).

2-17 C. Zener, "Theory of Do for Atomic Diffusion in Metals", J. Appl. Phys. 22, 372 (1951).

2-18 C. H. Fellows, J. Amer, Water Wks. Ass. 21, 1373 (1929).

2-19 F. A. Champion, Corrosion Testing Procedures, 2d ed., (Wiley, New York, 1965).

2-20 E. A. Gulbransen, and K. F. Andrew, J. Electrochem. Soc. 97, 383 (1950).

2-21 E. C. Potter and G. M. W. Mann, "Oxidation of Mild Steel in High-Temperature Aqueous Systems", in First International Congress on Metallic Corrosion, London, April 1961 (Butterworths, London, 1962).

2-22 E. A. Gulbransen, "The Transition State Theory of the Formation of Thin Oxide Films on Metals", Trans. Electrochem. Soc. 83, 301 (1943).

2-23 W. W. Smeltzer, "Oxidation of Aluminum in the Temperature Range 400-600°C", J. Electrochem. Soc. 103, 209 (1956).

2-24 J.S.L. Leach, "Some Characteristics of Protective Oxide Films", in Proceedings of the Second International Congress on Metallic Corrosion, New York, March 1963, (National Association of Corrosion Engineers, Houston, 1966.)

2-25 H. H. Uhlig, "Effect of Metal Composition and Structure on Corrosion and Oxidation", in Proceedings of the Second International Congress on Metallic Corrosion, New York, March 1963, (National Association of Corrosion Engineers, Houston, 1966).

2-26 W. J. Moore, "Oxidation of Metals at High Temperature", J. Electrochem. Soc. 100, 302 (1953).

2-27 W. S. C. cott, and J. C. Whetzel, "Laboratory Corrosion Tests", ans. Smer. Inst. Chem. Eng. 15, 1 (1923).

Section 3.0:

3-1 D. K. Edwards, G. L. Fleischman and B. D. Marcus, "User's
     Manual for the TRW Gaspipe Program", NASA CR-114306,
     April 1971, and "User's Manual for the TRW Gaspipe 2
     Program", NASA CR-114672, October 1973.

3-2 D. K. Edwards, G. L. Fleischman, B. D. Marcus, "User's
     Manual for the TRW GASPIPE 2 Program", TRW Report No.
     13111-6054-R0-00, October 1973.

Section 4.0:

4-1 F. Edelstein, J. G. Roukis and J. D. Loose, "The Develop-
     ment of a 150,000 watt-inch Variable Conductance Heat
     Pipe for Space Vehicle Thermal Control", ASME Paper No.
     72-ENAv-14, 1973.

7.0 NOMENCLATURE

Section 2:

A   -   Area

B   -   Multiplicative constant

k   -   Boltzmann's constant

n   -   Number of moles

P_g -   Partial pressure of gas

P_v -   Partial pressure of vapor

Q   -   Activation energy

R   -   Gas constant

T   -   Temperature

t   -   Time

V   -   Volume

$(\ )_a$-   Refers to adiabatic section

$(\ )_c$-   Refers to transition from parabolic to linear time dependence

$(\ )_i$-   Refers to i^{th} interval

$(\ )_1$-   Refers to passivation period

$(\ )_2$-   Refers to period beyond passivation

Section 4:

A_c -   Cross-sectional vapor area in condenser

B   -   Constant

c   -   Specific heat

D   -   Diffusion coefficient

g   -   Gravitational constant

h_{fg}-   Latent heat

L_c -   Condenser length

m   -   Mass

M   -   Molecular weight

N   -   Number of moles

P   -   Pressure (also perimeter of heat-transfer area)

Q   -   Heat

R   -   Thermal resistance of condenser

    -   Universal gas constant

T   -   Temperature

t   -   Time

U - Heat-transfer coefficient

V - Total gas-blocked volume

Z - Length of active portion of condenser

ζ - Complex coefficient of t in exponent of assumed solution (Eq. (4-5)].

α, ω - Real and imaginary parts of ζ

τ_p, τ_d - Constants (dimensions of time)

τ - Time lag

ρ - Density

$(\ )_a$- Refers to adiabatic section

$(\ )_c$- Refers to condenser section

$(\ )_e$- Refers to evaporator section

$(\cdot)$ - Time rate

8.0   APPENDIX

The Tables of Content of previous research reports follow.
Research Reports Nos. 1 & 2 can also be found combined in Ref. [1-3].

THEORY AND DESIGN
OF VARIABLE CONDUCTANCE
HEAT PIPES: HYDRODYNAMICS
AND HEAT TRANSFER

Research Report No. 1

APRIL 1971

Prepared by

B.D. MARCUS

Prepared for

AMES RESEARCH CENTER
NATIONAL AERONAUTICS AND SPACE ADMINISTRATION
Moffett Field, California 93405

TRW
SYSTEMS GROUP

ONE SPACE PARK • REDONDO BEACH CALIFORNIA 50278

TABLE OF CONTENTS

THEORY AND DESIGN
OF VARIABLE CONDUCTANCE
HEAT PIPES:
CONTROL TECHNIQUES

Research Report No. 2

JULY 1971

Prepared by

B.D. MARCUS

Prepared for

TRW

SYSTEMS GROUP

TABLE OF CONTENTS

THEORY AND DESIGN OF VARIABLE CONDUCTANCE HEAT PIPES: STEADY STATE AND TRANSIENT PERFORMANCE

PREPARED BY
D. K. EDWARDS
G. L FLEISCHMAN
B. D. MARCUS

TABLE OF CONTENTS

VARIABLE CONDUCTANCE
HEAT PIPE
TECHNOLOGY

Research Report No. 4

DECEMBER 1973

Prepared by

B.D. MARCUS
D.K. EDWARDS
W.T. ANDERSON

Contract No. NAS 2-5503

ᴵ

TABLE OF CONTENTS

AMES HEAT PIPE EXPERIMENT (AHPE) EXPERIMENT DESCRIPTION DOCUMENT

PREPARED BY

B. D. MARCUS

CONTRACT NO. NAS 2-5503

PREPARED FOR
NASA—AMES RESEARCH CENTER
MOFFET FIELD, CALIFORNIA 93405

TABLE OF CONTENTS